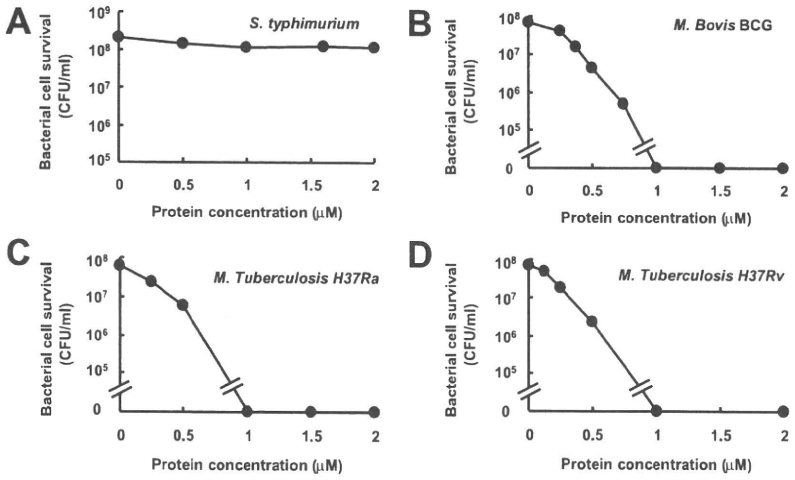

FIGURE 2. Mouse recombinant SLPI inhibits in vitro BCG and *M. tuberculosis* growth. *A*, *S. typhimurium* (5×10^7 CFU/ml) were incubated with SLPI for 2 h and plated on LB agar plates. *B–D*, BCG (*B*), *M. tuberculosis* H37Ra (*C*), or *M. tuberculosis* H37Rv (*D*; 5×10^7 CFU/ml) were incubated with increasing concentrations of recombinant mouse SLPI for 24 h and then plated on 7H10 agar plates.

Bronchoalveolar lavage fluid (BALF)

Mice were intratracheally administered 4×10^5 CFU of BCG suspended in 30 μl of PBS. BALF was collected at the indicated periods. To obtain alveolar macrophages, BALF was centrifuged at 2000 × g for 2 min and the pellet was resuspended in RPMI 1640 containing 4% FBS. The cell count of alveolar macrophages was $\sim 1 \times 10^5$ cells/mouse. To eliminate contamination by bacteria, alveolar macrophages were cultured with 50 U/ml penicillin and 50 μg/ml streptomycin for 16 h, washed five times, and infected with 5×10^7 CFU/well of BCG without penicillin and streptomycin.

Preparation of recombinant SLPI protein and variants

PCR-amplified mouse SLPI cDNA fragments were inserted into pGEX-6P-1 (Amersham Biosciences). pGEX-6P-1 containing mouse SLPI cDNA was transformed into *Escherichia coli* Rosetta-gami B (DE 3). Expression of GST-SLPI fusion proteins was induced by the addition of 1 mM isopropyl-1-thio-β-D-galactoside, and the expressed fusion proteins were purified using glutathione-Sepharose 4B (Amersham Biosciences) according to the manufacturer's instructions. The purified proteins were incubated with PreScission Protease (Amersham Biosciences) at 4°C for 16 h to cleave the GST tag and then purified with glutathione-Sepharose 4B.

Antibacterial activity

Mid-log phase *Salmonella typhimurium* were diluted with PBS containing 1% Luria-Bertani (LB) to give $\sim 5 \times 10^7$ CFU/ml. A final volume of 250 μl was used to examine the antibacterial activities of proteins. After incubation for 2 h, *S. typhimurium* were plated onto LB agar plates. Colonies were counted (CFU/ml) after overnight incubation at 37°C.

Antimycobacterial activity

M. tuberculosis and BCG were grown in Middlebrook 7H9-ADC medium at 37°C with vigorous agitation. After 7 days of incubation, rapidly growing mycobacteria were harvested by centrifugation and adjusted to 5×10^7 CFU/ml in 7H9-ADC medium. After incubation of the mycobacteria with the indicated concentrations of proteins for 24 h at 37°C, serial 20-fold dilutions were conducted in PBS. Aliquots (50 μl) of the dilutions were plated on Middlebrook 7H10 agar plates and incubated at 37°C for 21–28 days. Colonies were counted (CFU/ml) at intervals until no new colonies appeared.

Protein-binding assay

SLPI and BSA were labeled with 5-(and 6-)carboxyfluorescein-*N*-hydroxysuccinimide ester (FLUOS; Roche Diagnostics) as described previously (30). Briefly, 400 μg/ml SLPI or BSA was mixed with 0.096 mg of FLUOS in 1 ml of PBS for 2 h at room temperature. Nonreacted FLUOS was separated by gel filtration using a Sephadex G25 column (Amersham Biosciences). The labeled SLPI or BSA was then incubated with BCG, and the OD at 630 nm was adjusted to 0.2. After 30 min of incubation at 37°C, BCG were washed three times with 7H9 medium containing 0.05% Tween 80. Protein-BCG reactions were detected by confocal laser microscopy (Zeiss).

Scanning electron microscopy

After culture with or without 1 μM SLPI for the indicated times, BCG cultures were fixed with 5% glutaraldehyde, postfixed with 1% osmium tetroxide, dehydrated with ethyl alcohol, treated with isoamyl acetate to replace the alcohol, dried with liquid CO_2 in a critical-point apparatus (HCP-2; Hitachi), and coated with Pt-Pd by ion sputtering (Hitachi) in ion-distilled water. The specimens were analyzed using S-4700 scanning electron microscope (Hitachi), operated at 10 kV.

Outer membrane permeabilization assay

The ability of proteins to permeabilize the outer membranes of BCG was investigated using 1-*N*-phenylnaphthylamine (NPN; Wako Pure Chemical Industries) as described previously (31). Briefly, BCG were suspended in 5 mM HEPES (pH 7.4) containing 10 μM NPN to an OD at 590 nm of 0.15. After incubation at 37°C for 30 min, proteins were added and the fluorescence of NPN was monitored. The excitation wavelength used was 340 nm, and the emission wavelength was 425 nm. The experiment was conducted at 37°C.

Generation of $Slpi^{-/-}$ *mice*

The *Slpi* gene was isolated from genomic DNA extracted from embryonic stem cells (E14.1) by PCR using TaKaRa LA *Taq*. The targeting vector was constructed by replacing a 1.2-kb fragment containing exons 2–4 with a neomycin-resistance gene cassette (*neo*) driven by the PGK promoter and inserting a HSV thymidine kinase into the genomic fragment for negative selection. After transfection of the targeting vector into embryonic stem cells, colonies resistant to both G418 and ganciclovir were selected and screened by PCR and Southern blotting. Homologous recombinants were microinjected into blastocysts of C57BL/6 female mice and heterozygous F_1 progenies were intercrossed to obtain $Slpi^{-/-}$ mice.

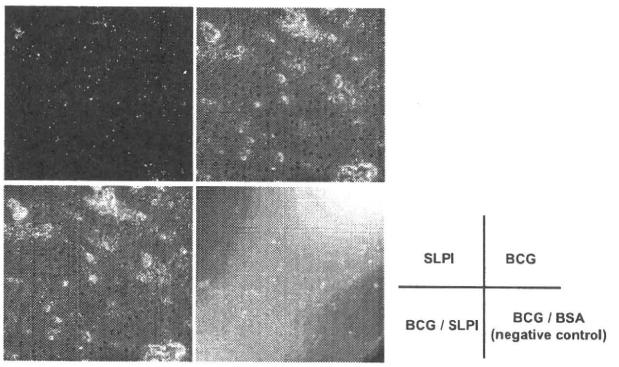

FIGURE 3. SLPI associates with BCG. SLPI and BSA were labeled with FLUOS (Roche). Labeled proteins were incubated with BCG for 30 min, and analyzed by fluorescence microscopy.

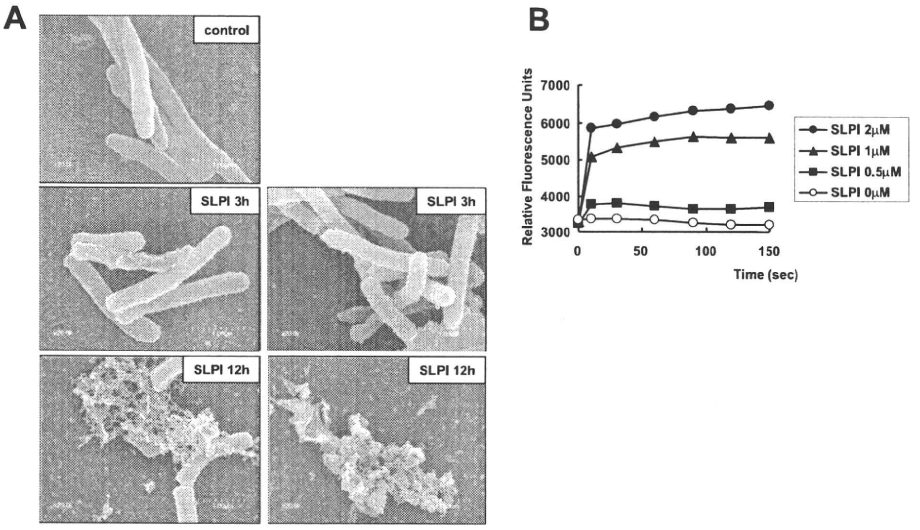

FIGURE 4. SLPI disrupts the BCG cell membrane. *A*, BCG was incubated with or without SLPI for the indicated periods and observed with scanning electron microscopy. *B*, The indicated concentrations of SLPI were added to a BCG suspension containing NPN, and the NPN fluorescence was monitored for the indicated periods. Representative data of three independent experiments are shown.

Slpi$^{-/-}$ mice were backcrossed to C57BL/6 mice for five generations, and *Slpi*$^{-/-}$ and their wild-type littermates from these intercrosses were used for experiments at 6–8 wk of age. All animal experiments were conducted in accordance with the guidelines of the Animal Care and Use Committee of Kyushu University.

In vivo infection

For intratracheal infection, 4×10^5 CFU of *M. tuberculosis* suspended in 30 μl of sterile PBS were administered intratracheally. For i.v. infection, 4×10^5 CFU of *M. tuberculosis* suspended in 100 μl of sterile PBS were administered i.v. At 3 wk after infection, homogenates of the lungs and spleen were plated on 7H10 agar plates. For histological examination, 1×10^7 CFU of *M. tuberculosis* suspended in 30 μl of sterile PBS were administered intratracheally. At 5 days after infection, the lungs were fixed in 4% formalin, embedded in paraffin, cut into sections, and stained with H&E.

Results

SLPI expression in the lungs of BCG-infected mice

To assess the roles of SLPI in mycobacterial infection, we first analyzed SLPI expression in the lungs of mice intratracheally infected with *M. bovis* BCG. Total RNA was extracted from the lungs after 2, 7, and 14 days of infection and analyzed for SLPI mRNA expression by real-time qPCR (Fig. 1*A*). Expression of SLPI mRNA was increased by ~9-fold after 2 days of infection, but decreased thereafter. Next, we analyzed pulmonary cell types expressing SLPI by immunohistochemical analysis (Fig. 1, *B* and *C*). SLPI was detected in bronchial epithelial cells before BCG infection (Fig. 1*B, upper micrograph*). After 2 days of BCG infection, increased amounts of SLPI expression were observed, and mainly localized at the apical side of bronchial epithelial cells (Fig. 1*B, lower micrograph*). This prompted us to investigate whether SLPI was secreted into the alveolar space after BCG infection. Accordingly, BALF was collected from BCG-infected mice and analyzed for SLPI protein expression by Western blotting (Fig. 1*D*). SLPI was not detected in BALF from uninfected mice. After 2 days of BCG infection, SLPI was abundantly detected in BALF from infected mice, indicating that SLPI was secreted into the alveolar space during the early phase of mycobacterial infection. In addition to bronchial epithelial cells, SLPI was expressed in cells of the alveolar area (Fig. 1*C*). Therefore, we isolated type II alveolar epithelial cells (AEC) and alveolar macrophages and analyzed their SLPI expression levels after BCG infection. Since AEC are difficult to culture in vitro, we took advantage of transgenic mice harboring a temperature-sensitive mutation of the SV40 large tumor Ag gene under the control of an IFN-γ-inducible H-2K^b promoter element (32, 33). Using these mice, we successfully established AEC lines expressing surfactant protein C (data not shown).

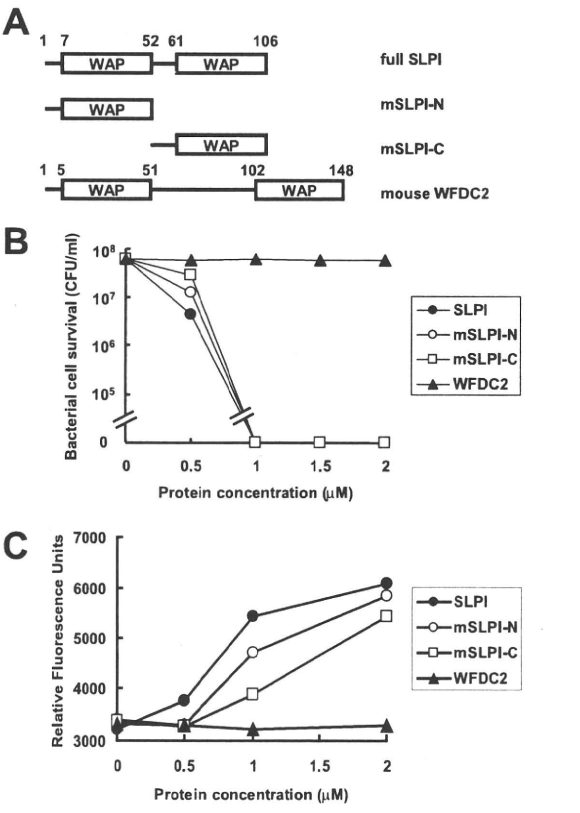

FIGURE 5. A single WAP domain in SLPI is sufficient to inhibit BCG growth. *A*, The deletion mutant constructs mSLPI-N and mSLPI-C lack the C-terminal and N-terminal portions, respectively. White boxes denote WAP domains. *B*, BCG (5×10^7 CFU/ml) was incubated with increasing concentrations of the deletion mutants (mSLPI-N and mSLPI-C) or WFDC2 for 24 h and then plated on 7H10 agar plates. *C*, The indicated concentrations of the deletion mutants (mSLPI-N and mSLPI-C) or WFDC2 were added to BCG suspensions containing NPN. The peak of NPN fluorescence within 150 s was plotted. Representative data of three independent experiments are shown.

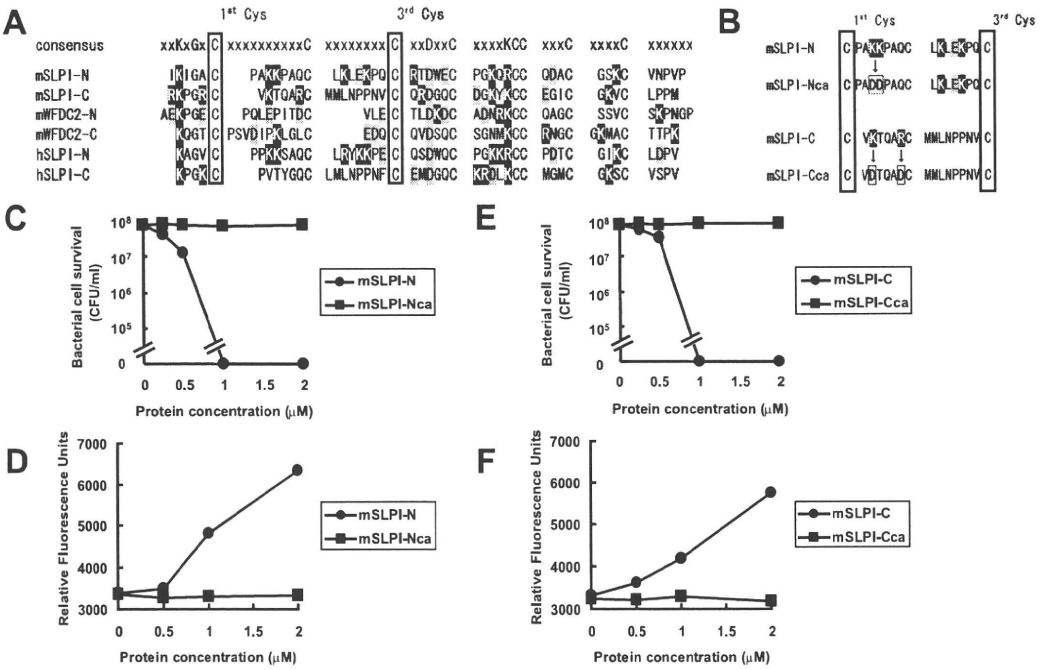

FIGURE 6. Cationic amino acids are responsible for the antimycobacterial activity of SLPI. *A*, Comparison of the WAP domain of SLPI with the WAP domains of other proteins. The consensus amino acid sequence of the WAP domain is shown at the *top* of the protein sequences. Black- and gray-boxed amino acids indicate cationic and anionic amino acids, respectively. Two conserved cysteine residues (first cysteine and third cysteine) are boxed. *B*, Amino acid sequences of the mSLPI-N (mSLPI-Nca) and mSLPI-C (mSLPI-Cca) mutants. *C* and *E*, BCG (5×10^7 CFU/ml) was incubated with increasing concentrations of mSLPI-Nca (*C*) and mSLPI-Cca (*E*) for 24 h and then plated on 7H10 agar plates. *D* and *F*, The indicated concentrations of mSLPI-Nca (*D*) and mSLPI-Cca (*F*) were added to BCG cultures containing NPN. The peak of NPN fluorescence within 150 s was plotted.

AEC were infected with BCG and analyzed for SLPI mRNA expression (Fig. 1*E*). SLPI mRNA expression was gradually induced after BCG infection and peaked after 36 h of infection. AEC have the ability to secrete several effector molecules into the alveolar space. Therefore, we analyzed the SLPI protein levels in culture supernatants from BCG-infected AEC by Western blotting (Fig. 1*F*). SLPI protein was not detected in supernatants from uninfected AEC, but was clearly detected in supernatants after 24 h of BCG infection. Next, isolated alveolar macrophages were infected with BCG and analyzed for SLPI mRNA expression (Fig. 1*G*). BCG infection resulted in an increase in SLPI mRNA expression. Taken together, mycobacterial infection induces the production and secretion of SLPI into the alveolar space by bronchial and type II alveolar epithelial cells as well as alveolar macrophages in the lung.

SLPI-mediated inhibition of mycobacterial growth

Several previous reports have described antimicrobial activities of SLPI against Gram-positive bacteria, Gram-negative bacteria, HIV, and fungi (18–20). However, SLPI needs to be present at high concentrations (>10 μM) for effective inhibition of microbial growth, particularly *S. typhimurium* and *E. coli* (18, 34). Indeed, addition of 2 μM recombinant mouse SLPI only moderately decreased the growth of *S. typhimurium* (Fig. 2*A*). In sharp contrast to the mild inhibition of *S. typhimurium* growth, addition of lower concentrations of mouse SLPI to BCG cultures dramatically reduced the number of CFU (Fig. 2*B*). Growth of BCG was almost completely inhibited by the addition of 1 μM SLPI. A similar inhibitory effect was observed on the growth of *M. tuberculosis* H37Ra and H37Rv (Fig. 2, *C* and *D*). These findings indicate that SLPI has a more potent antimicrobial activity against mycobacteria than against *S. typhimurium*.

Disruption of the BCG cell wall structure by SLPI

Next, we investigated the mechanism of the antimycobacterial activity of SLPI. First, fluorescence-labeled SLPI was incubated with BCG and analyzed by confocal laser microscopy (Fig. 3). BCG and labeled SLPI were colocalized, suggesting that SLPI becomes associated with BCG. We then examined the morphological effects of SLPI on BCG. BCG was incubated with or without SLPI and analyzed by scanning electron microscopy (Fig. 4*A*). BCG exposed to SLPI for 3 h showed pronounced surface blebbing. After 12 h of incubation, many of BCG were collapsed and few live BCG had rough and irregular membrane surfaces. Next, BCG was subjected to an outer membrane permeabilization assay using a fluorescent dye that is weakly fluorescent in aqueous environments but becomes strongly fluorescent in the hydrophobic environment within the cell membrane (Fig. 4*B*). Addition of SLPI caused rapid increases in fluorescence in a dose-dependent manner. These results suggest that SLPI directly associates with mycobacteria, and disrupts the cell wall structure.

Critical role of cationic amino acids in SLPI in its antimycobacterial activity

We next investigated the critical domain involved in the antimycobacterial activity of SLPI. SLPI has two WAP domains (Fig. 5*A*). Several serine protease inhibitors possessing a single WAP domain, such as Eppin, Elafin, SWAM1, and SWAM2, have antimicrobial activities against bacteria such as *E. coli* and *Staphylococcus aureus* (8, 21, 22). To investigate whether each of the WAP domains of mouse SLPI is sufficient to exert antimycobacterial activity, two deletion mutants of SLPI, mSLPI-N and

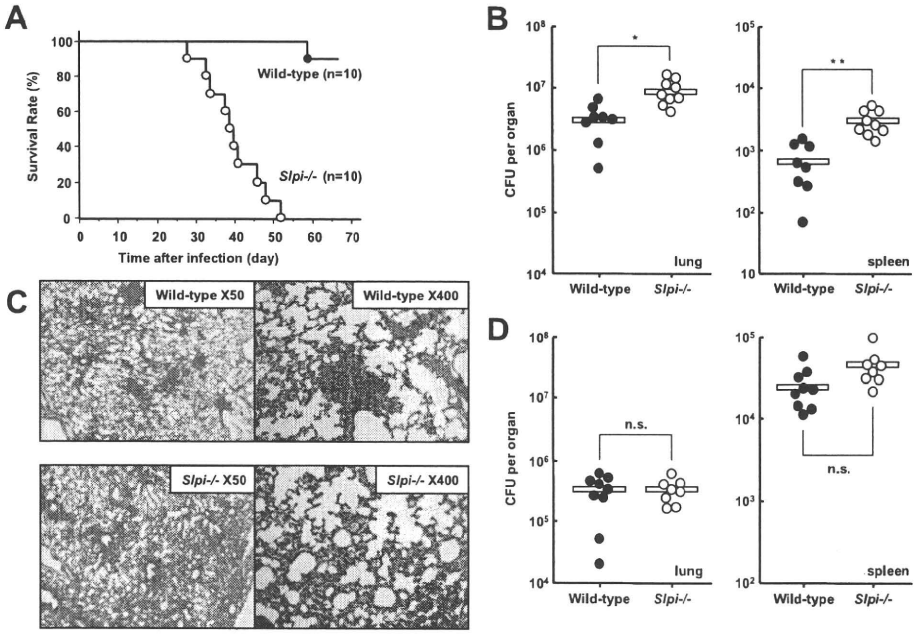

FIGURE 7. $Slpi^{-/-}$ mice are highly susceptible to *M. tuberculosis* infection. *A*, *M. tuberculosis* (4×10^5 CFU) were intratracheally infected into wild-type and $Slpi^{-/-}$ mice and their survival was monitored. *B*, *M. tuberculosis* (4×10^5 CFU) were intratracheally infected into wild-type and $Slpi^{-/-}$ mice. At 3 wk after infection, homogenates of the lungs and spleen were plated on 7H10 agar plates and the CFU titers were counted. Symbols represent individual mice and bars represent the mean of CFU numbers. Statistical analyses were performed using Student's *t* test: *, $p < 0.005$ and **, $p < 0.0005$, significant difference between wild-type and $Slpi^{-/-}$ mice. *C*, H&E staining of representative lung tissues from wild-type and $Slpi^{-/-}$ mice on day 5 after intratracheal infection with *M. tuberculosis*. *D*, *M. tuberculosis* (4×10^5 CFU) were i.v. infected into wild-type and $Slpi^{-/-}$ mice. At 3 wk after infection, homogenates of the lungs and spleen were plated on 7H10 agar plates, and the CFU titers were counted. Symbols represent individual mice and bars represent the mean of CFU numbers. Statistical analyses were performed using Student's *t* test. n.s., Not significant.

mSLPI-C, were generated (Fig. 5*A*). mSLPI-N contained the N-terminal WAP domain, while mSLPI-C contained the C-terminal WAP domain. Both mSLPI-N and mSLPI-C inhibited BCG growth, although their efficiencies were slightly decreased compared with that of full-length SLPI (Fig. 5*B*). Similarly, mSLPI-N and mSLPI-C both induced permeabilization of the outer membrane of BCG with slightly lower efficacies (Fig. 5*C*). These results imply that each WAP domain of mouse SLPI exhibits antimycobacterial activity by disrupting the mycobacterial cell wall structure. WFDC2 is a secreted protein possessing two WAP domains (Fig. 5*A*) (35). However, recombinant mouse WFDC2 had no effect on mycobacterial growth and did not induce permeabilization of the BCG cell membrane, indicating that not all WAP domain-containing proteins have antimicrobial activities (Fig. 5, *B* and *C*). In addition, the N-terminal, but not the C-terminal, WAP domain of human SLPI has been shown to mediate its antimicrobial activities against *E. coli* and *S. aureus* (18). Therefore, we compared the amino acid sequences of the WAP domains of mouse and human SLPI as well as mouse WFDC2 (Fig. 6*A*). The C-terminal regions were conserved among all of the WAP domains. However, the sequences between the first and third cysteine residues were less conserved. In particular, when we examined the sequences between the first and second cysteine residues, we noted that the WAP domains possessing antimycobacterial activities (mSLPI-N, mSLPI-C, and hSLPI-N) contained two or more cationic amino acids, whereas the WAP domains with no antimycobacterial activities (mWFDC2-N, mWFDC2-C, and hSLPI-C) had one or zero cationic acids and instead contained anionic amino acids. Therefore, we produced mSLPI-N (mSLPI-Nca) and mSLPI-C (mSLPI-Cca) mutants, in which the two cationic amino acids were changed to the anionic amino acid aspartic acid (Fig. 6*B*). Neither mSLPI-Nca nor mSLPI-Cca was able to inhibit BCG growth or permeabilize the cell membrane (Fig. 6, *C–F*). These results suggest that the cationic acids of mouse SLPI are responsible for its potent antimycobacterial activities.

High susceptibility of SLPI-deficient mice to M. tuberculosis *infection*

In the next experiment, we assessed the physiological roles of SLPI during mycobacterial infection by generating mice lacking SLPI ($Slpi^{-/-}$ mice) via gene targeting (data not shown). First, wild-type and $Slpi^{-/-}$ mice were intratracheally infected with *M. tuberculosis* H37Ra, and monitored for their survival (Fig. 7*A*). All $Slpi^{-/-}$ mice died within 8 wk of infection at a dose that almost all wild-type mice survived for >9 wk. Next, we counted CFU numbers in the lungs and spleen after 3 wk of infection (Fig. 7*B*). The CFU titers of *M. tuberculosis* in both tissues were higher for $Slpi^{-/-}$ mice than that for wild-type mice. The histopathological changes in the lungs after 5 days of *M. tuberculosis* infection were also analyzed (Fig. 7*C*). In wild-type mice, the formation of several small granulomas was observed. In contrast, granulomatous changes were induced to a lesser extent in $Slpi^{-/-}$ mice and rather diffuse cell infiltration was observed instead. Next, mice were i.v. infected with *M. tuberculosis*, and the CFU numbers in the lungs and spleen were counted after 3 wk of infection (Fig. 7*D*). The CFU titers were not as dramatically increased in both tissues of $Slpi^{-/-}$ mice compared with the corresponding titers in the tissues of wild-type mice, indicating that $Slpi^{-/-}$ mice are not highly susceptible to i.v. *M. tuberculosis* infection. Taken together, these findings indicate that $Slpi^{-/-}$ mice are highly vulnerable to *M. tuberculosis* infection via the respiratory route.

Discussion

In the present study, we analyzed the roles of mouse SLPI in host defense against mycobacteria. During the early phase of respiratory mycobacterial infection, SLPI was produced and secreted into the alveolar space by bronchial and type II alveolar epithelial cells as well as alveolar macrophages. Recombinant mouse SLPI inhibited the growth of mycobacteria more effectively than it inhibited the growth of Gram-negative bacteria. The SLPI-mediated inhibition of mycobacterial growth was attributable to disruption of the mycobacterial cell wall structure. Furthermore, *Slpi*$^{-/-}$ mice were highly susceptible to pulmonary *M. tuberculosis* infection, highlighting a mandatory role for mouse SLPI in the host defense against *M. tuberculosis* infection. Thus, mouse SLPI is a critical antimycobacterial molecule that acts during the early phase of mycobacterial infection at the respiratory mucosal surface.

Similar structural changes to those observed in SLPI-treated mycobacterial cell walls were induced in several bacteria and *M. tuberculosis* treated with the antimicrobial peptides defensins, which permeabilize microbial membranes (36, 37). We further identified the critical elements for the potent antimycobacterial activity of mouse SLPI. It has been proposed that defensins containing positively charged amino acid residues associate with microorganisms by targeting the surface-exposed negatively charged phospholipid head groups in the microbial membrane (37). Indeed, mutations that change arginine to aspartic acid can attenuate the bactericidal activity of the α-defensin cryptdin-4 (38). Therefore, we supposed that SLPI, which has similar effects on mycobacterial membranes to defensins, also associates with negatively charged mycobacterial membranes through its positively charged amino acid residues. Consistent with this hypothesis, the sequences between the first and second conserved cysteine residues of the WAP domains are not conserved. Moreover, there are several positively charged amino acids (lysine and arginine) in these regions of the WAP domains that possess antimicrobial activities, whereas the regions without any antimicrobial activities contain one or zero positively charged amino acids. Furthermore, structural studies have revealed that the region between the first and second conserved cysteine residues is exposed on the outside of the molecule, thereby enabling this region to associate with microbial membranes (39, 40). Indeed, mutations of the cationic amino acid residues within this region resulted in elimination of the antimycobacterial activity. Thus, mouse SLPI exhibits antimycobacterial activity in quite a similar manner to that of defensins.

In comparison to SLPI, higher concentrations of other serine protease inhibitors containing a WAP domain are required to inhibit microbial growth (8, 21, 22). Recombinant human SLPI is less effective at inhibiting the growth of mycobacteria and *S. typhimurium* (our unpublished data). These differential properties may be attributable to structural differences in the WAP domains, which mediate the antimicrobial activity. SLPI has two WAP domains, whereas other serine protease inhibitors, such as Eppin, Elafin, and SWAMs, have only a single WAP domain. In the case of human SLPI, only the N-terminal WAP domain exhibits antimicrobial activity (18). In addition, only the N-terminal WAP domain of human SLPI contains critical cationic acid residues. The presence of two WAP domains possessing antimicrobial activity may be responsible for the high potency of mouse SLPI for mycobacterial growth inhibition.

Mouse SLPI inhibited mycobacterial growth at profoundly lower concentrations than those required to inhibit the growth of *S. typhimurium* or other microorganisms (18–20). It remains unclear how SLPI becomes more specifically targeted toward mycobacteria. Differential antimicrobial properties against distinct microorganisms have not been reported in the case of defensins. Therefore, SLPI, which has multifunctional properties, may have an unknown strategy for specifically recognizing mycobacteria.

The in vitro findings demonstrating that mouse SLPI inhibits mycobacterial growth were further strengthened by in vivo studies using *Slpi*$^{-/-}$ mice. *Slpi*$^{-/-}$ mice were highly susceptible to pulmonary *M. tuberculosis* infection, but not to i.v. infection. In accordance with this finding, SLPI protein was abundantly detected in the alveolar space after pulmonary BCG infection, but was not detected in sera from mice after i.v. BCG infection (our unpublished data). Therefore, high concentrations of SLPI are supposed to be secreted into the alveolar space during the early phase of respiratory infection with *M. tuberculosis*, thereby promptly killing the mycobacteria before they can invade the lung tissues through the epithelial barrier. Given that mouse SLPI has potent antimycobacterial activities, it would be a good candidate for treatment during the acute phase of *M. tuberculosis* infection and may even be able to be used for the treatment of patients with multidrug-resistant *M. tuberculosis*.

Acknowledgments

We thank S. Ehrt and A. Ding for helpful discussions, Y. Yamada and K. Takeda for technical assistance, and M. Kurata for secretarial assistance.

Disclosures

The authors have no financial conflict of interest.

References

1. Kaufmann, S. H. 2006. Tuberculosis: back on the immunologists' agenda. *Immunity* 24: 351–357.
2. North, R. J., and Y. J. Jung. 2004. Immunity to tuberculosis. *Annu. Rev. Immunol.* 22: 599–623.
3. Fremond, C. M., V. Yeremeev, D. M. Nicolle, M. Jacobs, V. F. Quesniaux, and B. Ryffel. 2004. Fatal *Mycobacterium tuberculosis* infection despite adaptive immune response in the absence of MyD88. *J. Clin. Invest.* 114: 1790–1799.
4. Quesniaux, V., C. Fremond, M. Jacobs, S. Parida, D. Nicolle, V. Yeremeev, F. Bihl, F. Erard, T. Botha, M. Drennan, et al. 2004. Toll-like receptor pathways in the immune responses to mycobacteria. *Microbes Infect.* 6: 946–959.
5. Gerritsen, J. 2000. Host defence mechanisms of the respiratory system. *Paediatr. Respir. Rev.* 1: 128–134.
6. Clauss, A., H. Lilja, and A. Lundwall. 2005. The evolution of a genetic locus encoding small serine proteinase inhibitors. *Biochem. Biophys. Res. Commun.* 333: 383–389.
7. Eisenberg, S. P., K. K. Hale, P. Heimdal, and R. C. Thompson. 1990. Location of the protease-inhibitory region of secretory leukocyte protease inhibitor. *J. Biol. Chem.* 265: 7976–7981.
8. Hagiwara, K., T. Kikuchi, Y. Endo, Huqun, K. Usui, M. Takahashi, N. Shibata, T. Kusakabe, H. Xin, S. Hoshi, et al. 2003. Mouse SWAM1 and SWAM2 are antibacterial proteins composed of a single whey acidic protein motif. *J. Immunol.* 170: 1973–1979.
9. Abe, T., N. Kobayashi, K. Yoshimura, B. C. Trapnell, H. Kim, R. C. Hubbard, M. T. Brewer, R. C. Thompson, and R. G. Crystal. 1991. Expression of the secretory leukoprotease inhibitor gene in epithelial cells. *J. Clin. Invest.* 87: 2207–2215.
10. Hiemstra, P. S., S. van Wetering, and J. Stolk. 1998. Neutrophil serine proteinases and defensins in chronic obstructive pulmonary disease: effects on pulmonary epithelium. *Eur. Respir. J.* 12: 1200–1208.
11. Schiessler, H., E. Fink, and H. Fritz. 1976. Acid-stable proteinase inhibitors from human seminal plasma. *Methods Enzymol.* 45: 847–859.
12. Vogelmeier, C., R. C. Hubbard, G. A. Fells, H. P. Schnebli, R. C. Thompson, H. Fritz, and R. G. Crystal. 1991. Anti-neutrophil elastase defense of the normal human respiratory epithelial surface provided by the secretory leukoprotease inhibitor. *J. Clin. Invest.* 87: 482–488.
13. Wingens, M., B. H. van Bergen, P. S. Hiemstra, J. F. Meis, I. M. van Vlijmen-Willems, P. L. Zeeuwen, J. Mulder, H. A. Kramps, F. van Ruissen, and J. Schalkwijk. 1998. Induction of SLPI (ALP/HUSI-I) in epidermal keratinocytes. *J. Invest. Dermatol.* 111: 996–1002.
14. Gauthier, F., U. Fryksmark, K. Ohlsson, and J. G. Bieth. 1982. Kinetics of the inhibition of leukocyte elastase by the bronchial inhibitor. *Biochim. Biophys. Acta* 700: 178–183.
15. Thompson, R. C., and K. Ohlsson. 1986. Isolation, properties, and complete amino acid sequence of human secretory leukocyte protease inhibitor, a potent inhibitor of leukocyte elastase. *Proc. Natl. Acad. Sci. USA* 83: 6692–6696.
16. Ashcroft, G. S., K. Lei, W. Jin, G. Longenecker, A. B. Kulkarni, T. Greenwell-Wild, H. Hale-Donze, G. McGrady, X. Y. Song, and S. M. Wahl. 2000. Secretory leukocyte protease inhibitor mediates non-redundant functions necessary for normal wound healing. *Nat. Med.* 6: 1147–1153.

17. Zhu, J., C. Nathan, W. Jin, D. Sim, G. S. Ashcroft, S. M. Wahl, L. Lacomis, H. Erdjument-Bromage, P. Tempst, C. D. Wright, and A. Ding. 2002. Conversion of proepithelin to epithelins: roles of SLPI and elastase in host defense and wound repair. *Cell* 111: 867–878.
18. Hiemstra, P. S., R. J. Maassen, J. Stolk, R. Heinzel-Wieland, G. J. Steffens, and J. H. Dijkman. 1996. Antibacterial activity of antileukoprotease. *Infect. Immun.* 64: 4520–4524.
19. McNeely, T. B., D. C. Shugars, M. Rosendahl, C. Tucker, S. P. Eisenberg, and S. M. Wahl. 1997. Inhibition of human immunodeficiency virus type 1 infectivity by secretory leukocyte protease inhibitor occurs prior to viral reverse transcription. *Blood* 90: 1141–1149.
20. Tomee, J. F., P. S. Hiemstra, R. Heinzel-Wieland, and H. F. Kauffman. 1997. Antileukoprotease: an endogenous protein in the innate mucosal defense against fungi. *J. Infect. Dis.* 176: 740–747.
21. Simpson, A. J., A. I. Maxwell, J. R. Govan, C. Haslett, and J. M. Sallenave. 1999. Elafin (elastase-specific inhibitor) has anti-microbial activity against Gram-positive and Gram-negative respiratory pathogens. *FEBS Lett.* 452: 309–313.
22. Yenugu, S., R. T. Richardson, P. Sivashanmugam, Z. Wang, M. G. O'Rand, F. S. French, and S. H. Hall. 2004. Antimicrobial activity of human EPPIN, an androgen-regulated, sperm-bound protein with a whey acidic protein motif. *Biol. Reprod.* 71: 1484–1490.
23. Jin, F. Y., C. Nathan, D. Radzioch, and A. Ding. 1997. Secretory leukocyte protease inhibitor: a macrophage product induced by and antagonistic to bacterial lipopolysaccharide. *Cell* 88: 417–426.
24. Taggart, C. C., S. A. Cryan, S. Weldon, A. Gibbons, C. M. Greene, E. Kelly, T. B. Low, S. J. O'Neill, and N. G. McElvaney. 2005. Secretory leucoprotease inhibitor binds to NF-κB binding sites in monocytes and inhibits p65 binding. *J. Exp. Med.* 202: 1659–1668.
25. Taggart, C. C., C. M. Greene, N. G. McElvaney, and S. O'Neill. 2002. Secretory leucoprotease inhibitor prevents lipopolysaccharide-induced IκBα degradation without affecting phosphorylation or ubiquitination. *J. Biol. Chem.* 277: 33648–33653.
26. Nakamura, A., Y. Mori, K. Hagiwara, T. Suzuki, T. Sakakibara, T. Kikuchi, T. Igarashi, M. Ebina, T. Abe, J. Miyazaki, et al. 2003. Increased susceptibility to LPS-induced endotoxin shock in secretory leukoprotease inhibitor (SLPI)-deficient mice. *J. Exp. Med.* 197: 669–674.
27. Ding, A., H. Yu, J. Yang, S. Shi, and S. Ehrt. 2005. Induction of macrophage-derived SLPI by *Mycobacterium tuberculosis* depends on TLR2 but not MyD88. *Immunology* 116: 381–389.
28. Doi, T., H. Yamada, T. Yajima, W. Wajjwalku, T. Hara, and Y. Yoshikai. 2007. H2–M3-restricted $CD8^+$ T cells induced by peptide-pulsed dendritic cells confer protection against *Mycobacterium tuberculosis*. *J. Immunol.* 178: 3806–3813.
29. deMello, D. E., S. Mahmoud, P. J. Padfield, and J. W. Hoffmann. 2000. Generation of an immortal differentiated lung type-II epithelial cell line from the adult H-$2K^b$tsA58 transgenic mouse. *In Vitro Cell. Dev. Biol. Anim.* 36: 374–382.
30. Aoki, K., S. Matsumoto, Y. Hirayama, T. Wada, Y. Ozeki, M. Niki, P. Domenech, K. Umemori, S. Yamamoto, A. Mineda, et al. 2004. Extracellular mycobacterial DNA-binding protein 1 participates in mycobacterium-lung epithelial cell interaction through hyaluronic acid. *J. Biol. Chem.* 279: 39798–39806.
31. Loh, B., C. Grant, and R. E. Hancock. 1984. Use of the fluorescent probe 1-*N*-phenylnaphthylamine to study the interactions of aminoglycoside antibiotics with the outer membrane of *Pseudomonas aeruginosa*. *Antimicrob. Agents Chemother.* 26: 546–551.
32. Jat, P. S., M. D. Noble, P. Ataliotis, Y. Tanaka, N. Yannoutsos, L. Larsen, and D. Kioussis. 1991. Direct derivation of conditionally immortal cell lines from an H-$2K^b$-tsA58 transgenic mouse. *Proc. Natl. Acad. Sci. USA* 88: 5096–5100.
33. Whitehead, R. H., P. E. VanEeden, M. D. Noble, P. Ataliotis, and P. S. Jat. 1993. Establishment of conditionally immortalized epithelial cell lines from both colon and small intestine of adult H-$2K^b$-tsA58 transgenic mice. *Proc. Natl. Acad. Sci. USA* 90: 587–591.
34. Si-Tahar, M., D. Merlin, S. Sitaraman, and J. L. Madara. 2000. Constitutive and regulated secretion of secretory leukocyte proteinase inhibitor by human intestinal epithelial cells. *Gastroenterology* 118: 1061–1071.
35. Kirchhoff, C., I. Habben, R. Ivell, and N. Krull. 1991. A major human epididymis-specific cDNA encodes a protein with sequence homology to extracellular proteinase inhibitors. *Biol. Reprod.* 45: 350–357.
36. Miyakawa, Y., P. Ratnakar, A. G. Rao, M. L. Costello, O. Mathieu-Costello, R. I. Lehrer, and A. Catanzaro. 1996. In vitro activity of the antimicrobial peptides human and rabbit defensins and porcine leukocyte protegrin against *Mycobacterium tuberculosis*. *Infect. Immun.* 64: 926–932.
37. Zasloff, M. 2002. Antimicrobial peptides of multicellular organisms. *Nature* 415: 389–395.
38. Tanabe, H., X. Qu, C. S. Weeks, J. E. Cummings, S. Kolusheva, K. B. Walsh, R. Jelinek, T. K. Vanderlick, M. E. Selsted, and A. J. Ouellette. 2004. Structure-activity determinants in Paneth cell α-defensins: loss-of-function in mouse cryptdin-4 by charge-reversal at arginine residue positions. *J. Biol. Chem.* 279: 11976–11983.
39. Grutter, M. G., G. Fendrich, R. Huber, and W. Bode. 1988. The 2.5 A X-ray crystal structure of the acid-stable proteinase inhibitor from human mucous secretions analysed in its complex with bovine α-chymotrypsin. *EMBO J.* 7: 345–351.
40. Lin, C. C., and J. Y. Chang. 2006. Pathway of oxidative folding of secretory leucocyte protease inhibitor: an 8-disulfide protein exhibits a unique mechanism of folding. *Biochemistry* 45: 6231–6240.

JOURNAL OF BACTERIOLOGY, May 2008, p. 3613–3621 Vol. 190, No. 10
0021-9193/08/$08.00+0 doi:10.1128/JB.01850-07

Structural Analysis and Biosynthesis Gene Cluster of an Antigenic Glycopeptidolipid from *Mycobacterium intracellulare*▽†

Nagatoshi Fujiwara,[1]* Noboru Nakata,[2] Takashi Naka,[1,3] Ikuya Yano,[3] Matsumi Doe,[4] Delphi Chatterjee,[5] Michael McNeil,[5] Patrick J. Brennan,[5] Kazuo Kobayashi,[6] Masahiko Makino,[2] Sohkichi Matsumoto,[1] Hisashi Ogura,[7] and Shinji Maeda[8]

Department of Host Defense[1] and Virology,[7] Osaka City University Graduate School of Medicine, Osaka 545-8585, Japan; Department of Microbiology, Leprosy Research Center, National Institute of Infectious Diseases, Tokyo 189-0002, Japan[2]; Japan BCG Laboratory, Tokyo 204-0022, Japan[3]; Department of Chemistry, Graduate School of Science, Osaka City University, Osaka 558-8585, Japan[4]; Department of Microbiology, Immunology and Pathology, Colorado State University, Colorado 80523[5]; Department of Immunology, National Institute of Infectious Diseases, Tokyo 162-8640, Japan[6]; and Molecular Epidemiology Division, Mycobacterium Reference Center, The Research Institute of Tuberculosis, Japan Anti-Tuberculosis Association, Tokyo 204-8533, Japan[8]

Received 24 November 2007/Accepted 1 March 2008

***Mycobacterium avium-Mycobacterium intracellulare* complex (MAC) is the most common isolate of nontuberculous mycobacteria and causes pulmonary and extrapulmonary diseases. MAC species can be grouped into 31 serotypes by the epitopic oligosaccharide structure of the species-specific glycopeptidolipid (GPL) antigen. The GPL consists of a serotype-common fatty acyl peptide core with 3,4-di-*O*-methyl-rhamnose at the terminal alaninol and a 6-deoxy-talose at the *allo*-threonine and serotype-specific oligosaccharides extending from the 6-deoxy-talose. Although the complete structures of 15 serotype-specific GPLs have been defined, the serotype 16-specific GPL structure has not yet been elucidated. In this study, the chemical structure of the serotype 16 GPL derived from *M. intracellulare* was determined by using chromatography, mass spectrometry, and nuclear magnetic resonance analyses. The result indicates that the terminal carbohydrate epitope of the oligosaccharide is a novel *N*-acyl-dideoxy-hexose. By the combined linkage analysis, the oligosaccharide structure of serotype 16 GPL was determined to be 3-2′-methyl-3′-hydroxy-4′-methoxy-pentanoyl-amido-3,6-dideoxy-β-hexose-(1→3)-4-*O*-methyl-α-L-rhamnose-(1→3)-α-L-rhamnose-(1→3)-α-L-rhamnose-(1→2)-6-deoxy-α-L-talose. Next, the 22.9-kb serotype 16-specific gene cluster involved in the glycosylation of oligosaccharide was isolated and sequenced. The cluster contained 17 open reading frames (ORFs). Based on the similarity of the deduced amino acid sequences, it was assumed that the ORF functions include encoding three glycosyltransferases, an acyltransferase, an aminotransferase, and a methyltransferase. An *M. avium* serotype 1 strain was transformed with cosmid clone no. 253 containing *gtfB-drrC* of *M. intracellulare* serotype 16, and the transformant produced serotype 16 GPL. Together, the ORFs of this serotype 16-specific gene cluster are responsible for the biosynthesis of serotype 16 GPL.**

Mycobacterial diseases, such as tuberculosis and infection due to nontuberculous mycobacteria (NTM), are still among the most serious infectious diseases in the world. The incidence is increasing because of the spread of drug-resistant mycobacteria and the human immunodeficiency virus (HIV) infection/AIDS epidemic (16, 17, 30). *Mycobacterium avium-Mycobacterium intracellulare* complex (MAC) is the most common among isolates of NTM and is distributed ubiquitously in the environment. MAC causes pulmonary and extrapulmonary diseases in both immunocompromised and immunocompetent hosts. It affects primarily patients with advanced HIV infection. MAC includes at least two mycobacterial species, *M. avium* and *M. intracellulare*, that cannot be differentiated on the basis of traditional physical and biochemical tests (1, 41).

* Corresponding author. Mailing address: Department of Host Defense, Osaka City University Graduate School of Medicine, 1-4-3 Asahi-machi, Abeno-ku, Osaka 545-8585, Japan. Phone: 81 6 6645 3746. Fax: 81 6 6645 3747. E-mail: fujiwara@med.osaka-cu.ac.jp.

† Supplemental material for this article may be found at http://jb.asm.org/.

▽ Published ahead of print on 7 March 2008.

The cell envelope of mycobacteria is a complex and unusual structure. The key feature of this structure is an extraordinarily high lipid concentration (6, 10). To better understand the pathogenesis of MAC infection, it is necessary to elucidate the molecular structure and biochemical features of the lipid components. Among MAC lipids, the glycopeptidolipid (GPL) is of particular importance, because it shows not only serotype-specific antigenicity but also immunomodulatory activities in the host immune responses (2, 9, 23). Structurally, GPLs are composed of two parts, a tetrapeptide-amino alcohol core and a variable oligosaccharide (OSE). C_{26}-C_{34} fatty acyl-D-phenylalanine-D-*allo*-threonine-D-alanine-L-alaninol (D-Phe-D-*allo*-Thr-D-Ala-L-alaninol) is further linked with 6-deoxy talose (6-d-Tal) and 3,4-di-*O*-methyl rhamnose (3,4-di-*O*-Me-Rha) at D-*allo*-Thr and the terminal L-alaninol, respectively. This type of core GPL is found in all subspecies of MAC, shows a common antigenicity, and is further glycosylated at 6-d-Tal to form a serotype-specific OSE.

At present, 31 distinct serotype-specific GPLs have been identified serologically and chromatographically (9). Although the standard technique for differentiation of MAC subspecies

has been serotyping based on the OSE residue of its GPL, the complete structures of only 15 GPLs have been defined. In addition to the chemical structures of various GPLs, genes encoding the glycosylation pathways in the biosynthesis of GPL have been identified and characterized (12, 21, 31). Epidemiological studies have shown that MAC serotypes 4 and 8 are the most frequently isolated from patients, and MAC serotype 16 is one of the next most common groups (32, 40). It has been suggested that the serotypes of MAC isolates participate in their virulence (29), and thus, understanding of the structure-pathogenicity relationship of GPLs is necessary. In the present study, we demonstrate the complete OSE structure of the GPL derived from serotype 16 MAC (*M. intracellulare*), which has a unique terminal-acylated-amido sugar, and we characterized the serotype 16 GPL-specific gene cluster involved in the glycosylation of carbohydrates.

MATERIALS AND METHODS

Bacterial strains and preparation of GPL. *M. intracellulare* serotype 16 strain ATCC 13950^T (NF 115) was purchased from the American Type Culture Collection (Manassas, VA). Three clinical isolates of *M. intracellulare* serotype 16 (NF 116 and 117) and *M. avium* serotype 1 (NF 113) were maintained in The Research Institute of Tuberculosis, Japan Anti-Tuberculosis Association. The preparation of GPL was performed as described previously (18, 24, 26). Briefly, each strain of *M. intracellulare* serotype 16 was grown in Middlebrook 7H9 broth (Difco Laboratories, Detroit, MI) with 0.5% glycerol and 10% Middlebrook oleic acid-albumin-dextrose-catalase enrichment (Difco) at 37°C for 2 to 3 weeks. The heat-killed bacteria were sonicated, and crude lipids were extracted with chloroform-methanol (2:1, vol/vol). The extracted lipids were dried and hydrolyzed with 0.2 N sodium hydroxide in methanol at 37°C for 2 h. After neutralization with 6 N hydrochloric acid, alkaline-stable lipids were partitioned by a two-layer system of chloroform-methanol (2:1, vol/vol) and water. The organic phase was recovered, evaporated, and precipitated with acetone to remove any acetone-insoluble components containing phospholipids and glycolipids. The supernatant was collected by centrifugation, dried, and then treated with a Sep-Pak silica cartridge (Waters Corporation, Milford, MA) with washing (chloroform-methanol, 95:5, vol/vol) and elution (chloroform-methanol, 1:1, vol/vol) for partial purification. GPL was completely purified by preparative thin-layer chromatography (TLC) of Silica Gel G (20 by 20 cm, 250 μm; Uniplate; Analtech, Inc., Newark, DE). The TLC plate was repeatedly developed with chloroform-methanol-water (65:25:4 and 60:16:2, vol/vol/vol) until a single spot was obtained. After exposure of the TLC plate to iodine vapor, the GPL band was marked, and then, the silica gels were scraped off and the GPL was eluted with chloroform-methanol (2:1, vol/vol).

Preparation of OSE moiety. β elimination of GPL was performed with alkaline borohydride, and the OSE elongated from D-*allo*-Thr was released as described previously (18, 24). Briefly, the GPL was dissolved in ethanol, and an equal volume of 10 mg/ml sodium borohydride or borodeuteride in 0.5 N sodium hydroxide was added and then stirred at 60°C for 16 h. The reaction mixture was decationized with Dowex 50W-X8 beads (Dow Chemical Company, Midland, MI), collected, and evaporated under nitrogen to remove boric acid. The dried residue was partitioned in two layers of chloroform-methanol (2:1, vol/vol) and water. The upper aqueous phase was recovered and evaporated. In these processes, the serotype 16-specific OSE was purified as an oligoglycosyl alditol.

MALDI-TOF and MALDI-TOF/TOF MS analyses. The molecular species of the intact GPL was detected by matrix-assisted laser desorption ionization–time of flight mass spectrometry (MALDI-TOF MS) with an Ultraflex II (Bruker Daltonics, Billerica, MA). The GPL was dissolved in chloroform-methanol (2:1, vol/vol) at a concentration of 1 mg/ml, and 1 μl was applied directly to the sample plate, and then 1 μl of 10 mg/ml 2,5-dihydroxybenzoic acid in chloroform-methanol (1:1, vol/vol) was added as a matrix. The intact GPL was analyzed in the reflectron mode with an accelerating voltage operating in a positive mode of 20 kV (5). Then the fragment pattern of the OSE was analyzed with MALDI-TOF/TOF MS. The OSE was dissolved in ethanol-water (3:7, vol/vol), and the matrix was 10 mg/ml 2,5-dihydroxybenzoic acid in ethanol-water (3:7, vol/vol). The OSE and the matrix were applied to the sample plate according to the method for intact GPL and analyzed in the lift-lift mode.

GC and GC-MS analyses of carbohydrates and *N*-acylated short-chain fatty acid. To determine the glycosyl composition and linkage position, gas chromatography (GC) and GC-MS analyses of partially methylated alditol acetate derivatives were performed. Perdeuteromethylation was conducted by the modified procedure of Hakomori as described previously (18, 20). Briefly, the dried OSE was dissolved with a mixture of dimethyl sulfoxide and sodium hydroxide, and deuteromethyl iodide was added. The reaction mixture was stirred at room temperature for 15 min and then water and chloroform were added. The chloroform-containing perdeuteromethylated OSE layer was collected, washed with water two times, and then completely evaporated. Partially deuteromethylated alditol acetates were prepared from perdeuteromethylated OSE by hydrolysis with 2 N trifluoroacetic acid at 120°C for 2 h, reduction with 10 mg/ml sodium borodeuteride at 25°C for 2 h, and acetylation with acetic anhydride at 100°C for 1 h (8, 18, 25). To identify amino-linked fatty acids, acidic methanolysis of serotype 16 GPL was performed with 1.25 M hydrogen chloride in methanol (Sigma-Aldrich, St. Louis, MO) at 100°C for 90 min, and the fatty acid methyl esters were extracted with *n*-hexane under the cooled ice. GC was performed using a 5890 series II gas chromatograph (Hewlett Packard, Avondale, PA) equipped with a fused SPB-1 capillary column (30 m, 0.25-mm inner diameter; Supelco Inc., Bellefonte, PA). Helium was used for electron impact (EI)-MS and isobutane for chemical ionization (CI)-MS as a carrier gas. A JMS SX102A double-focusing mass spectrometer (JEOL, Tokyo, Japan) was connected to the gas chromatograph as a mass detector. The molecular separator and the ion source energy were 70 eV for EI and 30 eV for CI, and the accelerating voltage was 8 kV. The D and L configurations of Rha residues were determined by comparative GC-MS analysis of trimethylsilylated (*S*)-(+)-sec-butyl glycosides and (*R*)-(−)-sec-butyl glycosides prepared from an authentic standard L-Rha (19).

NMR analysis of GPL. The GPL was dissolved in chloroform-d ($CDCl_3$)-methanol-d_4 (CD_3OD) (2:1, vol/vol). To define the anomeric configurations of each glycosyl residue, ^1H and ^{13}C nuclear magnetic resonance (NMR) was employed. Both homonuclear correlation spectrometry (COSY) and ^1H-detected [^1H, ^{13}C] heteronuclear multiple-quantum correlation (HMQC) were recorded with a Bruker Avance-600 (Bruker BioSpin Corp., Billerica, MA), as described previously (9, 18, 24, 34).

Construction of *M. intracellulare* serotype 16 cosmid library. A cosmid library of *M. intracellulare* serotype 16 strain ATCC 13950^T was constructed as described previously (18). Bacterial cells were disrupted mechanically, and genomic DNA was extracted with phenol-chloroform and then precipitated with ethanol. Genomic DNA randomly sheared into 30- to 50-kb fragments in the extraction process was fractionated and electroeluted from agarose gels using a Takara Recochip (Takara, Kyoto, Japan). These DNA fragments were rendered blunt ended using T4 DNA polymerase and deoxynucleoside triphosphates and then were ligated to dephosphorylated arms of pYUB412 (XbaI-EcoRV and EcoRV-XbaI), which were the kind gifts of William R. Jacobs, Jr. (Department of Microbiology and Immunology, Albert Einstein College of Medicine, Bronx, NY). The cosmid vector pYUB412 is an *Escherichia coli-Mycobacterium* shuttle vector with the *int-attP* sequence for integration into a mycobacterial chromosome, *oriE* for replication in *E. coli*, a hygromycin resistance gene, and an ampicillin resistance gene. After in vitro packaging using Gigapack III Gold extracts (Stratagene, La Jolla, CA), recombinant cosmids were introduced into *E. coli* STBL2 [F$^-$ *mcrA* Δ(*mcrBC-hsdRMS-mrr*) *recA1 endA1 lon gyrA96 thi supE44 relA1* λ Δ(*lac-proAB*)] and stored at −80°C in 50% glycerol.

Isolation of cosmid clones carrying biosynthesis gene cluster of serotype 16 GPL and sequence analysis. Isolation of DNA from *E. coli* transductants was performed as described by Supply et al., with modifications (39). The colonies were picked, transferred to a 1.5-ml tube containing 50 μl of water, and then heated at 98°C for 5 min. After centrifugation at 14,000 rpm for 5 min, the supernatant was used as the PCR template. PCR was used to isolate cosmid clones carrying the rhamnosyltransferase (*rtfA*) gene with primers rtfA-F (5′-TTTTGGAGCGACGAGTTCATC-3′) and rtfA-R (5′-GTGTAGTTGACCACGCCGAC-3′). *rtfA* encodes an enzyme responsible for the transfer of Rha to 6-d-Tal in OSE (14, 31). The insert of cosmid clone no. 253 was sequenced using a BigDye Terminator, version 3.1, cycle sequencing kit (Applied Biosystems, Foster City, CA) and an ABI Prism 310 gene analyzer (Applied Biosystems). The putative function of each open reading frame (ORF) was identified by similarity searches between the deduced amino acid sequences and known proteins using BLAST (http://www.ncbi.nlm.nih.gov/BLAST/) and FramePlot (http://www.nih.go.jp/~jun/cgi-bin/frameplot.pl) with the DNASIS computer program (Hitachi Software Engineering, Yokohama, Japan).

Transformation of *M. avium* serotype 1 strain with cosmid clone no. 253. An *M. avium* serotype 1 strain (NF113) was transformed with pYUB412-cosmid clone no. 253 by electroporation, and hygromycin-resistant colonies were iso-

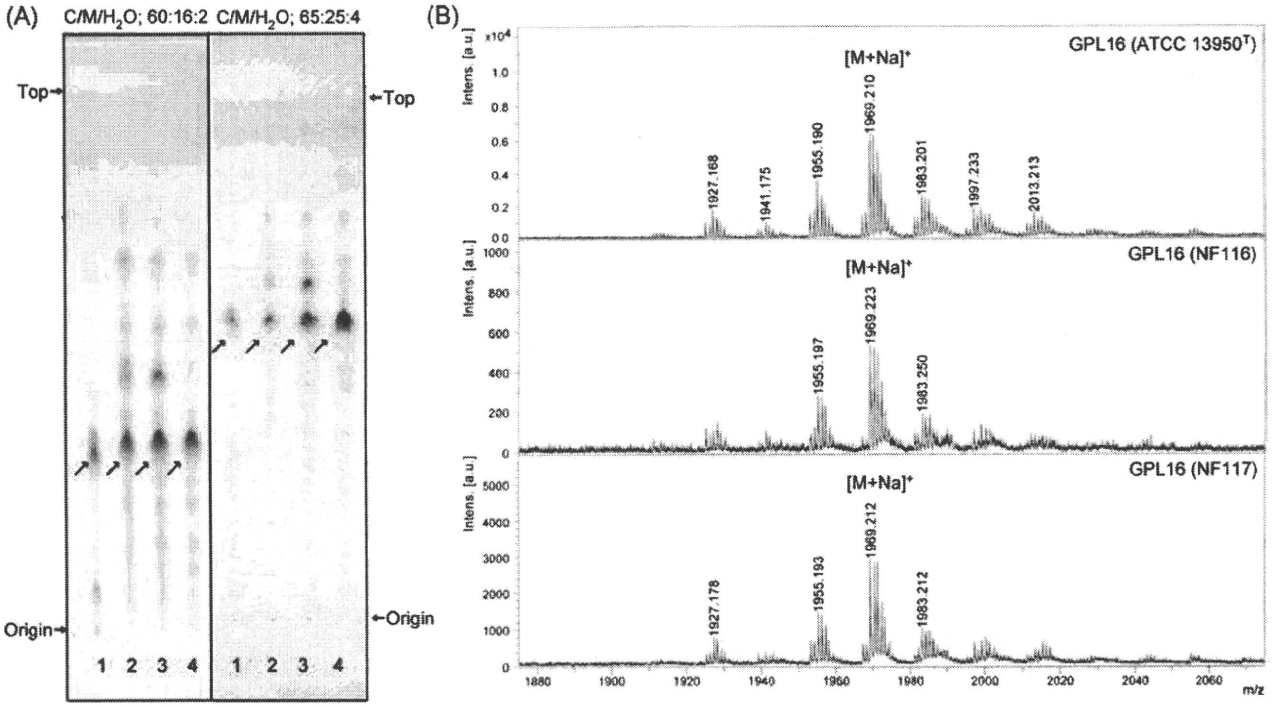

FIG. 1. TLC patterns and MALDI-TOF MS spectra of serotype 16 GPL. (A) Serotype 16 GPL purified from *M. intracellulare* ATCC 13950^T (NF 115) and the alkaline-stable lipids derived from ATCC 13950^T and two clinical isolates (NF 116 and 117) from left to right were developed on TLC plates with solvent systems of chloroform-methanol-water (65:25:4 and 60:16:2, vol/vol/vol). (B) The MALDI-TOF MS spectra were acquired using 10 mg/ml 2,5-dihydroxybenzoic acid in chloroform-methanol (1:1, vol/vol) as a matrix, and the molecularly related ions were detected as $[M+Na]^+$ in positive mode. Intens., intensity; a.u., absorbance units.

lated. Alkaline-stable lipids were prepared, and productive GPLs were examined by TLC and MALDI-TOF MS analyses.

Nucleotide sequence accession number. The nucleotide sequence reported here has been deposited in the NCBI GenBank database under accession no. AB355138.

RESULTS

Purification and molecular weight of intact GPL. Serotype 16 GPL from *M. intracellulare* ATCC 13950^T (NF 115) was detected as a spot by TLC, and the R_f values were 0.35 and 0.56 when developed with chloroform-methanol-water (60:16:2 and 65:25:4, vol/vol/vol, respectively). Two clinical isolates of *M. intracellulare*, NF 116 and 117, had serotype 16 GPLs that showed the same R_f values as the serotype 16 GPL derived from strain ATCC 13950^T. The serotype 16 GPL of *M. intracellulare* strain ATCC 13950^T was purified repeatedly by TLC and was shown as a single spot by TLC (Fig. 1A). The MALDI-TOF MS spectra of each serotype 16 GPL showed *m/z* 1969 for $[M+Na]^+$ as the main molecularly related ion in positive mode, with the homologous ions differing by 14 mass units at 1,955 and 1,983 (Fig. 1B). As a result, the main molecular weight of serotype 16 GPL was 1,946, which implied that it has a novel carbohydrate chain elongated from D-*allo*-Thr.

Carbohydrate composition of serotype 16 OSE. To determine the glycosyl compositions of serotype 16 OSE, alditol acetate derivatives of the serotype 16 GPL were analyzed by GC and GC-MS. The structurally defined serotype 4 GPL was used as a reference standard (9, 35). Comparison of the retention time and GC mass spectra (Fig. 2) with the alditol acetate derivatives of the serotype 16 GPL showed the presence of 3,4-di-*O*-Me-Rha, 4-*O*-Me-Rha, Rha, 6-d-Tal, and an unknown sugar residue (X1) in a ratio of approximately 1:1:2:1:1. The alditol acetate of X1 was eluted at a retention time of 29.3 min, greater than that of glucitol acetate on the SPB-1 column. The CI-MS spectrum of X1 was $[M+H]^+$ at *m/z* 520 as a parent ion and *m/z* 460 as a loss of 60 (acetate). The fragment ions of X1 sugar showed characteristic patterns in EI-MS. *m/z* 360 indicated the cleavage of C-3 and C-4, and *m/z* 300, 240, and 180 were fragmented with a loss of 60 (acetate). Similarly, *m/z* 374 indicated the cleavage of C-2 and C-3, and *m/z* 314 and 254 were fragmented with a loss of 60 (Fig. 3A and B). These results indicated that X1 was 3,6-dideoxy hexose (Hex). The odd molecular weight of X1, 519, and *m/z* 187, 127, and 59 implied the presence of one amido group esterified with a short-chain fatty acid, possibly. After methanolysis of serotype 16 GPL, the resultant fatty acid methyl esters were extracted carefully and analyzed by GC-MS. The EI-MS spectrum of a short-chain fatty acid methyl ester showed mass ions at *m/z* 176 ($[M]^+$), 145 ($[M-31]^+$), 117 ($[M-59]^+$), 99, 88, 85, and 59 (Fig. 3C) (33, 37). Taking the results together, X1 was structurally determined to be 3-2′-methyl-3′-hydroxy-4′-methoxy-pentanoyl-amido-3,6-dideoxy-Hex.

Glycosyl linkage and sequence of serotype 16 OSE. To determine the glycosyl linkage and sequence of the OSE, GC-MS of perdeuteromethylated alditol acetates and MALDI-TOF/TOF MS of the oligoglycosyl alditol from serotype 16 OSE

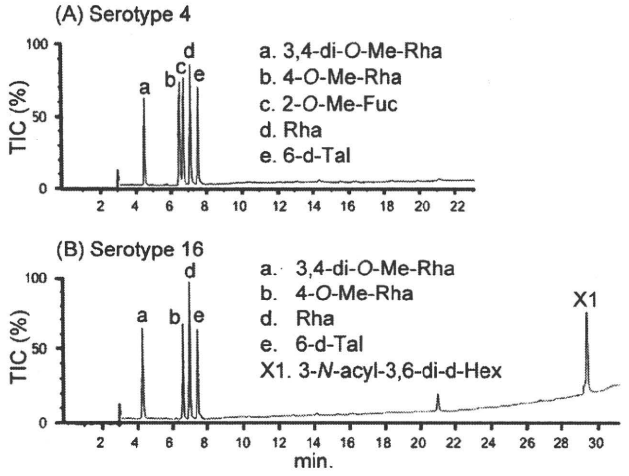

FIG. 2. Gas chromatograms of the alditol acetate derivatives from serotype 4 (A) and serotype 16 (B) GPLs. Total ion chromatograms (TIC) are shown. GC was performed on an SPB-1-fused silica column with a temperature program of 160°C for 2 min, followed by an increase of 4°C/min to 220°C, and holding at 220°C for 15 min. Comparison to the GC spectrum of serotype 4 GPL shows that serotype 16 GPL is composed of 3,4-di-*O*-Me-Rha, 4-*O*-Me-Rha, Rha, 6-d-Tal, and an unknown X1 sugar residue.

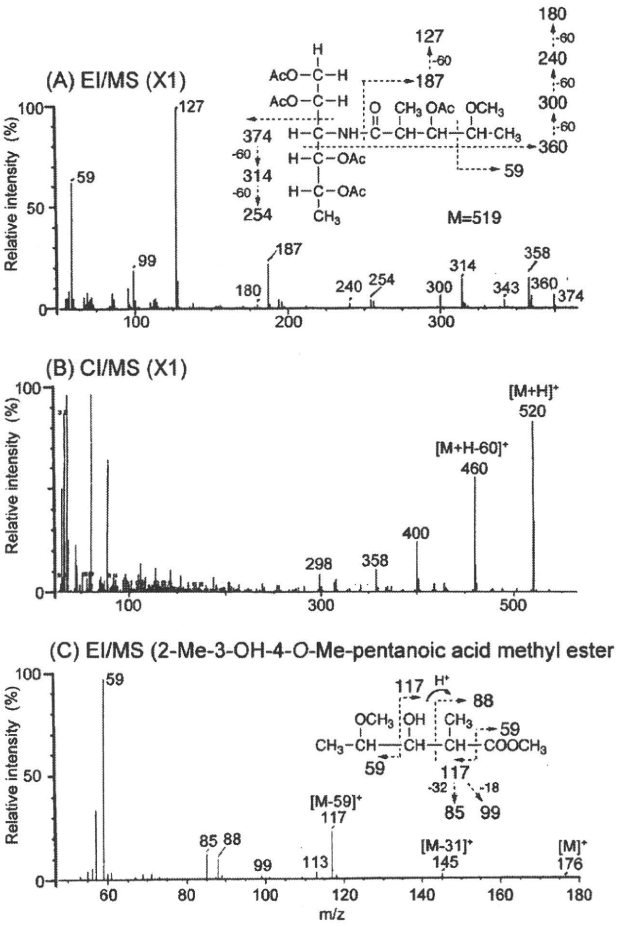

FIG. 3. EI-MS and CI-MS spectra of the alditol acetate derivative from X1 (A and B) and *N*-acylated-short-chain fatty acid methyl ester (C). The pattern of prominent fragment ions is illustrated. The CG column and condition were described in the legend for Fig. 2.

were performed. As shown in Fig. 4, the GC-MS spectra of perdeuteromethylated alditol acetates were assigned four major peaks, 1,3,4,5-tetra-*O*-deuteromethyl-2-*O*-acetyl-6-deoxy-talitol (*m/z* 109, 132, 154, 167, and 214); 2,4-di-*O*-deuteromethyl-1,3,5-tri-*O*-acetyl-rhamnitol (*m/z* 121, 134, 205, 240, and 253); 2-*O*-deuteromethyl-4-*O*-methyl-1,3,5-tri-*O*-acetyl-rhamnitol (*m/z* 121, 131, 202, and 237); and 2,4-di-*O*-deuteromethyl-1,5-di-*O*-acetyl-3-2′-methyl-3′-*O*-deuteromethyl-4′methoxy-pentanoyl-deuteromethylamido-3,6-dideoxy-hexitol (*m/z* 121, 134, and 341). These results revealed that the 6-d-Tal residue was linked at C-2; Rha and 4-*O*-Me-Rha were linked at C-1 and C-3; and the nonreducing terminus, 3-2′-methyl-3′-hydroxy-4′-methoxy-pentanoyl-amido-3,6-dideoxy-Hex, was C-1 linked. The MALDI-TOF/TOF MS spectrum of the oligoglycosyl alditol from serotype 16 OSE afforded the expected molecular ions $[M+Na]^+$ at *m/z* 931, together with the characteristic mass increments in the series of glycosyloxonium ions formed on fragmentation at *m/z* 312, 472, 618, and 764 from the terminal sugar *N*-acyl-Hex to 6-d-Tal and at *m/z* 336, 482, and 642 from 6-d-Tal to *N*-acyl-Hex (Fig. 5). Rha residues were determined to be in the L absolute configuration by comparative GC-MS analyses of trimethylsilylated (*S*)-(+)-sec-butyl glycosides and (*R*)-(−)-sec-butylglycosides (see Fig. S1 in the supplemental material). Taken together, these results established the sequence and linkage arrangement 3-2′-methyl-3′-hydroxy-4′-methoxy-pentanoyl-amido-3,6-dideoxy-Hex-(1→3)-4-*O*-Me-Rha-(1→3)-L-Rha-(1→3)-L-Rha-(1→2)-6-d-Tal, exclusively.

NMR analysis of serotype 16 OSE. The ^{1}H NMR and ^{1}H-^{1}H COSY analyses of the serotype 16 GPL revealed six distinct anomeric protons with corresponding H1-H2 cross peaks in the low field region at δ4.93, 4.92, 4.92, 4.84, 4.65 ($J_{1\text{-}2}$ = 2 to 3 Hz, indicative of α-anomers) and 4.51 (a doublet, $J_{1\text{-}2}$ = 7.7 Hz, indicative of a β-hexosyl unit). When further analyzed by ^{1}H-detected [^{1}H, ^{13}C] two-dimensional HMQC, the anomeric protons resonating at δ4.93, 4.92, 4.92, 4.84, 4.65, and 4.51 have C-1s resonating at δ101.57, 95.73, 101.40, 102.56, 100.97, and 103.36, respectively (for a summary, see Table S1 in the supplemental material). The J_{CH} values for each of these protons were calculated to be 171, 170, 171, 170, 169, and 161 Hz by measurement of the inverse-detection nondecoupled two-dimensional HMQC (Fig. 6). These results established that the terminal amido-Hex was a β configuration and the others were α-anomers.

Cloning and sequence of serotype 16 GPL biosynthesis cluster. To isolate the serotype 16 GPL biosynthesis cluster, the genomic cosmid library of *M. intracellulare* serotype 16 strain ATCC 13950^T was constructed. Primers were designed to amplify the region corresponding to the *rtfA* gene. More than 300 cosmid clones were tested using colony PCR with *rtfA* primers, and the positive clones no. 51 and 253 were isolated from the *E. coli* transductants. PCR analysis revealed that clone no. 253 contained a *drrC* gene but that clone no. 51 did not. Thus, we used clone no. 253 for subsequent sequence analysis for the *gtfB-drrC* region. The 22.9-kb region of *M. intracellulare* sero-

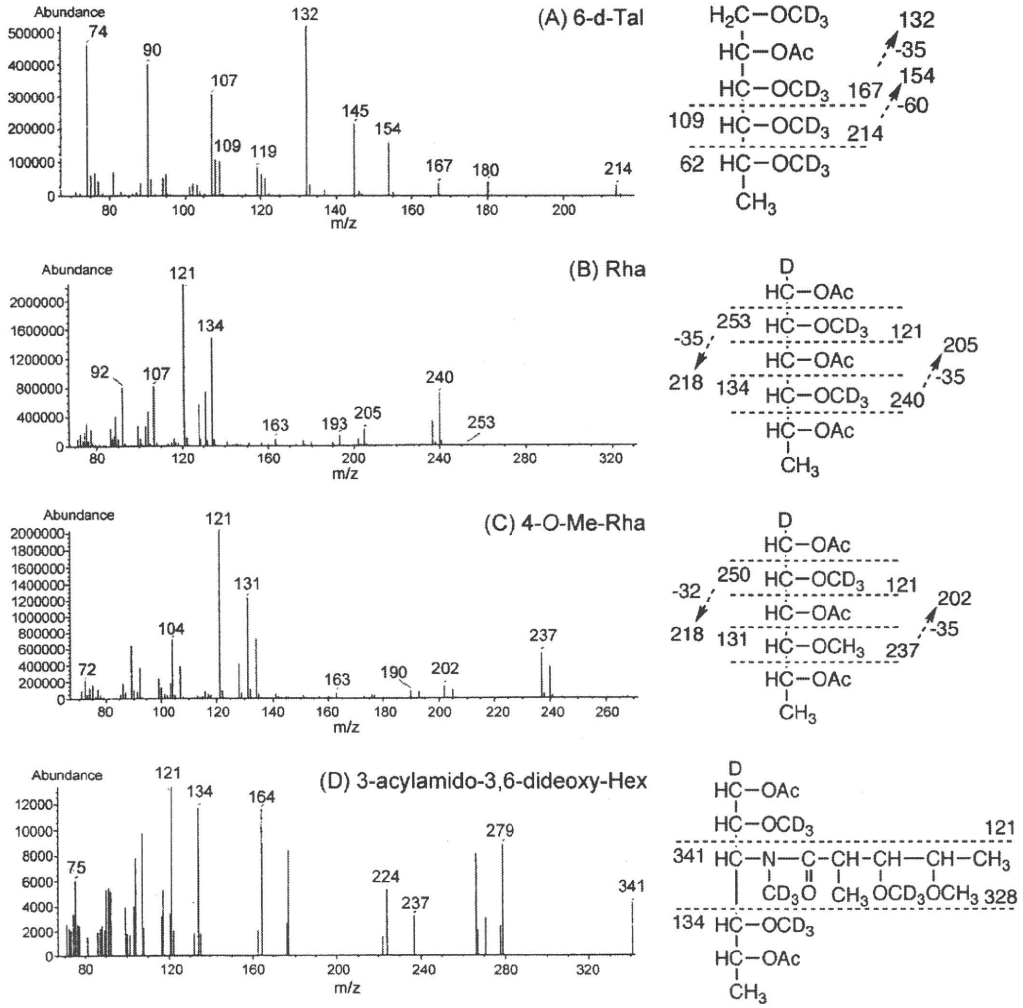

FIG. 4. GC-MS spectra of individual perdeuteromethylated alditol acetate derivatives from serotype 16 OSE. The formation of prominent fragment ions is illustrated; fragments were assigned to 1,3,4,5-tetra-*O*-deuteromethyl-2-*O*-acetyl-6-deoxy-talitol (A), 2,4-di-*O*-deuteromethyl-1,3,5-tri-*O*-acetyl-rhamnitol (B), 2-*O*-deuteromethyl-4-*O*-methyl-1,3,5-tri-*O*-acetyl-rhamnitol (C), and 2,4-di-*O*-deuteromethyl-1,5-di-*O*-acetyl-3-2′-methyl-3′-*O*-deuteromethyl-4′-methoxy-pentanoyl-deuteromethylamido-3,6-dideoxy-hexitol (D).

type 16 ATCC 13950^T was deposited in the NCBI GenBank database (accession no. AB355138). The similarity to protein sequences of each ORF is summarized in Table 1, and the genetic map for the serotype 16 GPL biosynthetic cluster was compared with those of serotype 2, 4, and 7 GPLs (Fig. 7). The *gtfB* and *drrC* genes of *M. intracellulare* serotype 16 ATCC 13950^T had 99.8% and 83.7% DNA identities with those of *M. intracellulare* serotype 7 ATCC 35847, respectively. In the DNA region between *gtfB* and *drrC* (20.8 kb), 17 ORFs were observed. Four ORFs (ORF 1, 2, 16, and 17) were homologous to those found in the same region of serotype 7-specific DNA, and the others were unique to the serotype 16 strain. No insertion of insertion elements or transposons was detected in this region. The nucleotide sequences of the ORF 1 and ORF 2 in serotype 16 strain ATCC 13950^T were homologous to those of ORF 1 and ORF 8 in serotype 7, respectively, suggesting that these two ORFs have the same function. The similarity of the deduced amino acid sequences suggested the possibility that the functions of ORF 3 and ORF 6 are to encode methyltransferase and aminotransferase, respectively. The deduced amino acid sequences of ORF 4 and ORF 5 showed significant similarities to the WxcM protein, the function of which is not clear. Interestingly, the deduced amino acid sequences of ORF 16 and ORF 17 of serotype 16 were homologous to ORF 9 of serotype 7. ORFs 1, 16, and 17 have considerable homology to glycosyltransferases. Nine ORFs, which are possibly involved in fatty acid synthesis, were detected between ORF 7 and ORF 15. It is notable that ORF 13 had a chimeric structure. The N-terminal half of ORF 13 showed similarity to phosphate butyryl/acetyl transferases, but the C-terminal half showed similarity to short-chain reductase/dehydrogenases. These results suggest that this region of DNA is responsible for the biosynthesis of the serotype 16-specific GPL.

Expression of cosmid clone no. 253 in *M. avium* serotype 1 strain. The OSE of serotype 1 GPL was composed of α-L-Rha-

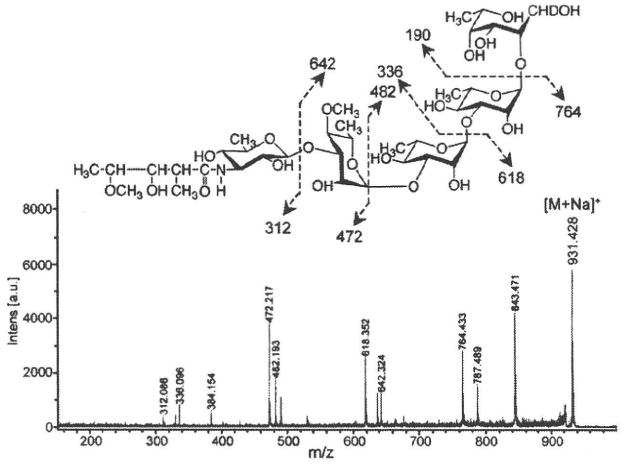

FIG. 5. MALDI-TOF/TOF MS spectrum of serotype 16 OSE. The formation of a characteristic increment in fragment ions is illustrated. The matrix was 10 mg/ml 2,5-dihydroxybenzoic acid in ethanol-water (3:7, vol/vol), and it was performed in the lift-lift mode. Intens., intensity; a.u., absorbance units.

(1→2)-6-d-L-Tal (9). The *M. avium* serotype 1 strain (NF113) was transformed with cosmid clone no. 253 containing a serotype 16-specific gene cluster and produced a new GPL with a different R_f value by TLC compared to serotype 1 GPL (Fig. 8A). The R_f value of the new GPL was identical to that of the serotype 16 GPL. The molecular weight of intact GPL, the fragment pattern of its OSE, and the GC pattern of the alditol acetate derivatives were completely equivalent to those of the serotype 16 GPL (see Fig. S2 in the supplemental material). As a result, the transformant of the serotype 1 strain expressed the cosmid clone no. 253 gene cluster and produced the serotype 16 GPL.

DISCUSSION

MAC species have serotype-specific GPLs that are characteristic components of the outer layer of the cell wall (6, 9). In addition to their serological differentiation, the chemical structures of 15 serotype-specific GPLs derived from the predominant clinical isolates have been analyzed; however, those of other GPLs remain unclear. The present study demonstrates the chemical structure of the serotype 16 GPL derived from *M. intracellulare*. We determined the glycosyl composition, linkage positions, and anomeric and ring configurations of the glycosyl residues of the serotype 16 GPL, and its OSE was defined as 3-2′-methyl-3′-hydroxy-4′-methoxy-pentanoyl-amido-3,6-dideoxy-β-Hex-(1→3)-4-*O*-methyl-α-L-Rha-(1→3)-α-L-Rha-(1→3)-α-L-Rha-(1→2)-6-d-α-L-Tal (Fig. 8B). The serotype 16 GPL should be listed as a group 2 polar GPL in the structural classification of Chatterjee and Khoo (9).

The GPLs of serotypes 7, 12, 17, and 19 have already been classified as group 2 GPLs, which are commonly composed of R→α-L-Rha-(1→3)-α-L-Rha-(1→2)-6-d-L-Tal (R, variable region), possessing a characteristic terminal sugar such as *N*-acyldeoxy-Hex. Indeed, the presence of an amido sugar has been reported in only five GPLs, serotypes 7, 12, 14, 17, and 25 (8, 9, 18). It has been determined that the OSE structure of the

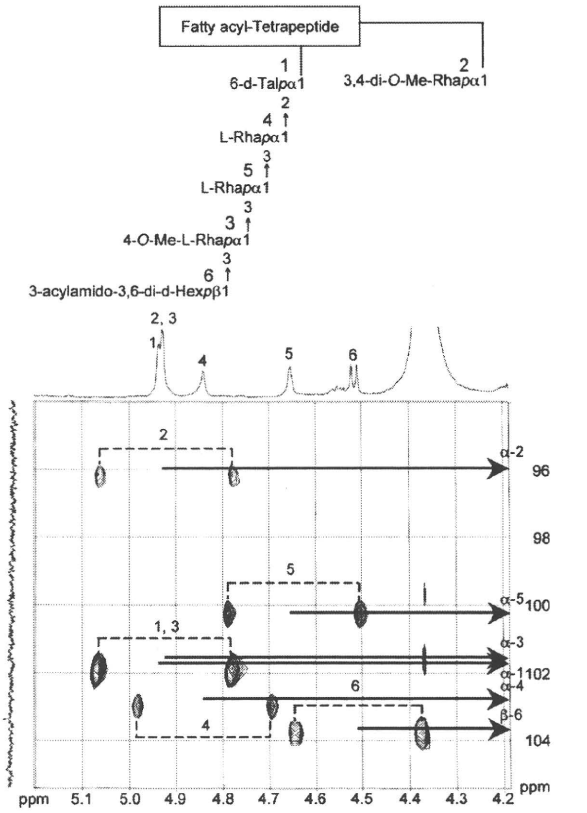

FIG. 6. Nondecoupled ^{1}H-detected [^{1}H, ^{13}C] HMQC spectrum of serotype 16 GPL. Cross-peak labels correspond to those shown on the structure.

serotype 17 GPL was 3-2′-methyl-3′-hydroxy-butanoyl-amido-3,6-dideoxy-β-D-Glc-(1→3)-4-*O*-methyl-α-L-Rha-(1→3)-α-L-Rha-(1→3)-α-L-Rha-(1→2)-6-d-L-Tal (9, 25). Based on the behavior of GPLs in TLC and the GC-MS analysis of alditol acetate derivatives, serotype 16 GPL seems to possess a unique carbohydrate epitope similar to that of serotype 17 GPL. We compared the OSE of serotype 16 GPL to that of serotype 17 GPL. The acylated amido group that was bound to the terminal sugar was different, although the linkage position was identical. Except for the terminal-acylated amido sugar, the other sugar compositions and glycosyl linkage positions were completely identical. An acylated amido group attached to the C-3 position of Hex is very unusual. To our knowledge, 3-amido-Hex is irregular in nature, although 2-amido-Hex is known to be glucosamine or galactosamine, which is frequently isolated as a component of lipopolysaccharides and glycosaminoglycans in prokaryotic and eukaryotic cells (7, 42). Further, existence of short-chain fatty acid 2-methyl-3-hydroxy-4-methoxy-pentanoic acid linked to the amido group of d-Hex is also unique. The characteristic gene cluster is thought to regulate the production of 3-acylated-amido-Hex. It is difficult to determine the species of acylated amido sugars, because no reference standard is available. The terminal sugar of the serotype 17 GPL was reviewed as a gluco-configuration, although firm evidence was not shown (9, 25). The J_{CH} and $J_{1\text{-}2}$ values for the anomeric proton in the terminal sugar were 161 and 7.7 Hz,

TABLE 1. Similarity to protein sequences of ORFs in cosmid clone no. 253 derived from *M. intracellulare* serotype 16 strain ATCC 13950^T

ORF	Predicted molecular mass (kDa)	Predicted pI	Exhibits similarity to:	E value	Amino acid identity (no. matched/total no.)	Accession no.
GtfB	45.6	6.35	Glycosyltransferase GtfB	0.0	417/418	BAF45360
Orf 1	45.2	6.10	Putative glycosyltransferase	0.0	416/417	BAF45361
Orf 2	78.9	8.51	Putative acyltransferase	0.0	557/728	BAF45368
Orf 3	31.0	5.88	Putative methyltransferase	2e-89	382/421	NP_218045
Orf 4	15.7	4.94	Conserved hypothetical protein	1e-39	73/129	BAD50406
Orf 5	16.0	4.69	Conserved hypothetical protein	5e-40	75/135	EAX55190
Orf 6	41.1	5.88	Aminotransferase/DegT_DnrJ_EryC1	6e-119	208/357	ABD68440
Orf 7	40.6	9.65	Conserved hypothetical protein	2e-89	178/304	AAS03547
Orf 8	36.7	5.32	Conserved hypothetical protein	2e-52	116/298	CAE06954
Orf 9	22.3	9.79	Putative *N*-acetyltransferase	4e-14	58/166	EAU11841
Orf 10	25.3	7.82	Short-chain dehydrogenase/reductase	7e-47	101/233	EAO61220
Orf 11	23.8	6.05	Putative hydrolase	4e-24	64/196	ABG85599
Orf 12	37.2	6.50	Ketoacyl-acyl carrier protein synthase III	3e-55	126/331	EAX48715
Orf 13	42.5	7.72	Short-chain dehydrogenase/reductase	2e-42	97/248	ZP_01289005
Orf 14	65.8	4.70	Predicted enzyme involved in methoxymalonyl-acyl carrier protein biosynthesis	6e-85	201/575	ABB73590
Orf 15	50.0	6.23	Acyl coenzyme A synthetases	2e-128	233/445	EAT27362
Orf 16	39.1	8.00	Putative glycosyltransferase	2e-106	196/318	NP_855197
Orf 17	37.7	9.46	Putative glycosyltransferase	8e-160	278/323	BAF45369
DrrC	28.6	11.47	Daunorubicin resistance protein C	6e-132	233/261	BAF45370

respectively (Fig. 6; Table S1 in the supplemental material). These results demonstrated unequivocally that the terminal amido-Hex was β configuration and H-2 was in the axial position. The terminal amido-Hex is considered to be derived from glucose or galactose, not Rha.

Next, we explored the genetic mechanism of GPL biosynthesis, because the elongation of carbohydrate chains in serotype-specific GPLs is poorly understood. The *ser2* gene cluster of the *M. avium* serotype 2 strain (31) and a 27.5-kb DNA fragment of the *M. avium* serotype 4 strain (28) were identified to be responsible for the biosynthesis of each OSE in GPLs. Recently, enzymatic characterizations of glycosyltransferase and methyltransferase of nonpolar GPLs have been reported for *Mycobacterium smegmatis* (36, 38). In the serotype-specific polar GPL biosynthesis of MAC, only the *rtfA* gene was functionally clarified to encode the transfer of L-Rha to 6-d-Tal, but which gene cluster transfers the sugars next to L-Rha elongated from 6-d-Tal is unclear.

In this study, we cloned the biosynthetic cluster of the serotype 16 GPL and analyzed its sequence. Seventeen ORFs were detected in the serotype 16 strain, and the sequence homology was analyzed. The transformant of the *M. avium* serotype 1

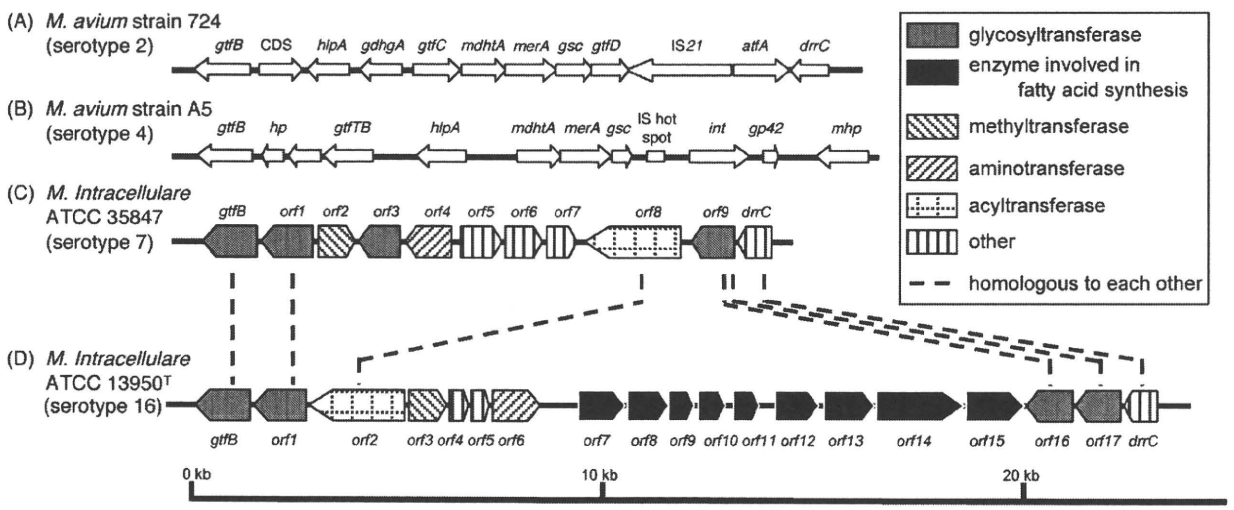

FIG. 7. Comparison and overview of genetic maps of GPL biosynthetic cluster. The *M. avium* strain 724 annotated sequence obtained from GenBank (accession no. AF125999) (A); the *M. avium* strain A5 annotated sequence obtained from GenBank (accession no. AY130970) (B); the *M. intracellulare* ATCC 35847 sequenced in our previous study (GenBank accession no. AB274811) (C); the *M. intracellulare* ATCC 13950^T sequenced in this study (GenBank accession no. AB355138) (D). The orientation of each gene is shown by the direction of the arrow. In panels A and B, putative ORFs not showing homology to known proteins sequences are not depicted. The sequences extending upstream in panels A and B and downstream in panel B are not included in the figure.

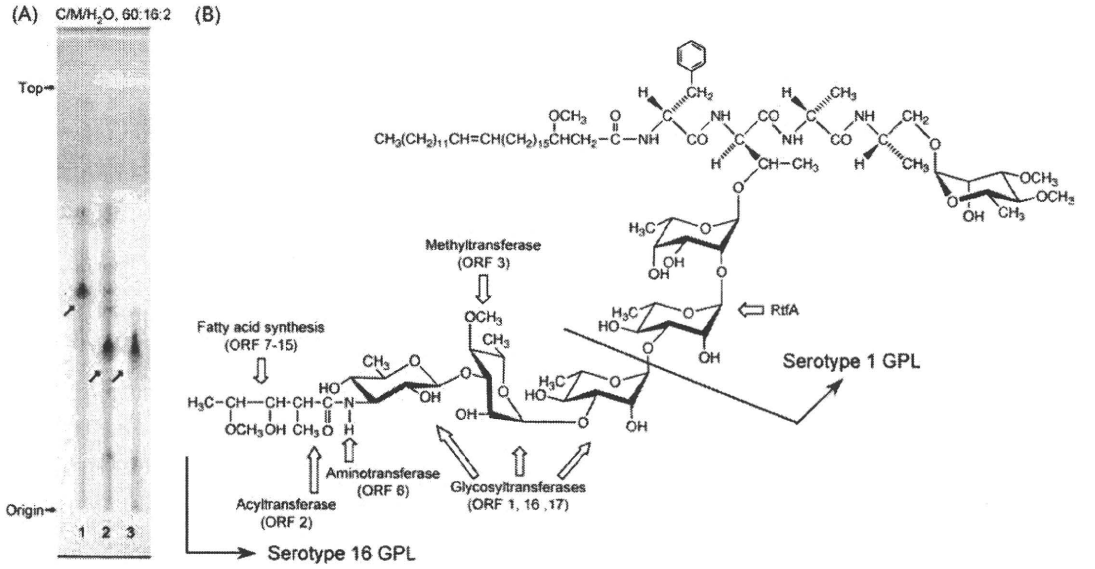

FIG. 8. TLC pattern of *M. avium* serotype 1 and its transformant with cosmid clone no. 253 and proposed complete structure of the serotype 16 GPL. (A) The alkaline-stable lipids derived from *M. avium* serotype 1 (lane 1), its transformant (lane 2), and purified serotype 16 GPL (lane 3) were developed with the solvent system of chloroform-methanol-water (60:16:2, vol/vol/vol). (B) Predicted biosynthesis gene clusters are indicated by arrows.

strain carrying cosmid clone no. 253 produced serotype 16 GPL. These results strongly implied that this *gtfB-drrC* region is responsible for the biosynthesis of the serotype 16-specific GPL. From the structural analysis of the serotype 16 GPL and the sequence of cosmid clone no. 253, it is possible to predict the relationship between the biosynthesis of serotype 16 GPL and the function of each ORF.

The genetic map of the serotype 16 GPL biosynthetic cluster was compared to those of serotype 2 GPL from *M. avium* strain 724, serotype 4 GPL from *M. avium* strain A5, and serotype 7 GPL from *M. intracellulare* strain ATCC 35847^T (12, 18, 28). Significant differences were found in the neighborhood of the conserved region. The genetic organization of the serotype 16 GPL gene cluster was distinct from that of serotype 7, except for some of the ORFs, and the ORFs in this region of serotype 2 and serotype 4 were completely different from ORFs 1 to 17 in serotype 16 (Fig. 7).

In addition to *M. intracellulare* serotype 7 (18) and serotype 16 strains, we have analyzed similar gene clusters of *M. intracellulare* serotype 12 and 17 strains. The sequence homology of the regions of ORF 1 and ORF 17 was highly conserved between only *M. intracellulare* serotype 16 and 17 strains (unpublished data). ORFs 1, 16, and 17 may lead to transfer of the two additional molecules of L-Rha and terminal amido-Hex. ORF 2 was assigned to acyltransferase and may be responsible for biosynthesis of the 3-2′-methyl-3′-hydroxy-4′-methoxy-pentanoyl-amido group in the terminal Hex. ORF 3 is probably responsible for the transfer of the *O*-methyl group at the C-4 position in the third L-Rha from 6-d-Tal. ORF 6 is homologous to aminotransferase and possibly associated with the biosynthesis of an amido group in the terminal Hex. The deduced amino acid sequences of ORF 6 in serotype 16 and ORF 4 in serotype 7 have homologies to DegT_DnrJ_EryC1 aminotransferases. However, these two ORFs are dissimilar to each other. Serotype 16 and 7 GPLs have an amido group at the terminal Hex, although the attachment position is different. The serotype 7 GPL has an amido group at the C-4 position in the terminal Hex, but the serotype 16 GPL has it at the C-3 position. Nine ORFs between ORF 7 and ORF 15 are possibly involved in fatty acid synthesis of the acyl chain moiety linked by an amido bond of the terminal Hex. Taken together, this gene cluster may participate in the biosynthetic pathway of the serotype 16-specific GPL, although further study is needed to clarify the function of each ORF.

Recent studies suggest that GPLs play an important role in the phenotype and pathogenicity of MAC. The colony morphology is considered to be influenced by cell wall GPL. MAC colony phenotypes spontaneously occur from smooth to rough type, and this is due to a mutation lacking GPL (3, 13, 22). The deletion of genomic regions encoding GPL biosynthesis may result in the loss of GPL. Danelishvili et al. demonstrated that the uptake by and growth in macrophages of a MAC mutant with the gene belonging to the GPL synthesis pathway inactivated by transposon insertion were decreased (11). Bhatnagar and Schorey have reported that macrophages infected with MAC release exosomes containing GPLs that result in the transfer of the GPLs to uninfected macrophages and induce a proinflammatory response (4). These findings imply that GPL participates in the pathogenicity of MAC. By contrast, our previous studies have demonstrated that anti-GPL antibodies are detected in the sera of most immunocompetent patients with MAC pulmonary disease and that the detection of anti-GPL antibody is useful for the serodiagnosis of MAC disease (15, 26, 27).

To understand the role of GPLs in MAC and its hosts, it is necessary to define the chemical structure and biosynthesis pathways of GPLs. Elucidation of the structure-function relationship of GPL may open a new avenue for controlling MAC disease.

ACKNOWLEDGMENTS

This work was supported by grants from the Ministry of Education, Culture, Sports, Science, and Technology of Japan, the Japan Health Sciences Foundation, and the Ministry of Health, Labor, and Welfare of Japan (Research on Emerging and Reemerging Infectious Diseases).

We are grateful to Sumihiro Hase (Department of Chemistry, Graduate School of Science, Osaka University, Osaka, Japan) and Hiromi Murakami (Osaka Municipal Technical Research Institute, Osaka, Japan) for helpful discussion.

REFERENCES

1. **Baess, I.** 1983. Deoxyribonucleic acid relationships between different serovars of *Mycobacterium avium*, *Mycobacterium intracellulare* and *Mycobacterium scrofulaceum*. Acta Pathol. Microbiol. Immunol. Scand. **91**:201–203.
2. **Barrow, W. W., T. L. Davis, E. L. Wright, V. Labrousse, M. Bachelet, and N. Rastogi.** 1995. Immunomodulatory spectrum of lipids associated with *Mycobacterium avium* serovar 8. Infect. Immun. **63**:126–133.
3. **Belisle, J. T., K. Klaczkiewicz, P. J. Brennan, W. R. Jacobs, Jr., and J. M. Inamine.** 1993. Rough morphological variants of *Mycobacterium avium*. Characterization of genomic deletions resulting in the loss of glycopeptidolipid expression. J. Biol. Chem. **268**:10517–10523.
4. **Bhatnagar, S., and J. S. Schorey.** 2007. Exosomes released from infected macrophages contain *Mycobacterium avium* glycopeptidolipids and are proinflammatory. J. Biol. Chem. **282**:25779–25789.
5. **Bhatt, A., N. Fujiwara, K. Bhatt, S. S. Gurcha, L. Kremer, B. Chen, J. Chan, S. A. Porcelli, K. Kobayashi, G. S. Besra, and W. R. Jacobs, Jr.** 2007. Deletion of *kasB* in *Mycobacterium tuberculosis* causes loss of acid-fastness and subclinical latent tuberculosis in immunocompetent mice. Proc. Natl. Acad. Sci. USA **104**:5157–5162.
6. **Brennan, P. J., and H. Nikaido.** 1995. The envelope of mycobacteria. Annu. Rev. Biochem. **64**:29–63.
7. **Campo, G. M., S. Campo, A. M. Ferlazzo, R. Vinci, and A. Calatroni.** 2001. Improved high-performance liquid chromatographic method to estimate aminosugars and its application to glycosaminoglycan determination in plasma and serum. J. Chromatogr. B **765**:151–160.
8. **Chatterjee, D., G. O. Aspinall, and P. J. Brennan.** 1987. The presence of novel glucuronic acid-containing, type-specific glycolipid antigens within *Mycobacterium* spp. Revision of earlier structures. J. Biol. Chem. **262**:3528–3533.
9. **Chatterjee, D., and K. H. Khoo.** 2001. The surface glycopeptidolipids of mycobacteria: structures and biological properties. Cell. Mol. Life Sci. **58**: 2018–2042.
10. **Daffe, M., and P. Draper.** 1998. The envelope layers of mycobacteria with reference to their pathogenicity. Adv. Microb. Physiol. **39**:131–203.
11. **Danelishvili, L., M. Wu, B. Stang, M. Harriff, S. Cirillo, J. Cirillo, R. Bildfell, B. Arbogast, and L. E. Bermudez.** 2007. Identification of *Mycobacterium avium* pathogenicity island important for macrophage and amoeba infection. Proc. Natl. Acad. Sci. USA **104**:11038–11043.
12. **Eckstein, T. M., J. T. Belisle, and J. M. Inamine.** 2003. Proposed pathway for the biosynthesis of serovar-specific glycopeptidolipids in *Mycobacterium avium* serovar 2. Microbiology **149**:2797–2807.
13. **Eckstein, T. M., J. M. Inamine, M. L. Lambert, and J. T. Belisle.** 2000. A genetic mechanism for deletion of the *ser2* gene cluster and formation of rough morphological variants of *Mycobacterium avium*. J. Bacteriol. **182**: 6177–6182.
14. **Eckstein, T. M., F. S. Silbaq, D. Chatterjee, N. J. Kelly, P. J. Brennan, and J. T. Belisle.** 1998. Identification and recombinant expression of a *Mycobacterium avium* rhamnosyltransferase gene (*rtfA*) involved in glycopeptidolipid biosynthesis. J. Bacteriol. **180**:5567–5573.
15. **Enomoto, K., S. Oka, N. Fujiwara, T. Okamoto, Y. Okuda, R. Maekura, T. Kuroki, and I. Yano.** 1998. Rapid serodiagnosis of *Mycobacterium avium-intracellulare* complex infection by ELISA with cord factor (trehalose 6, 6′-dimycolate), and serotyping using the glycopeptidolipid antigen. Microbiol. Immunol. **42**:689–696.
16. **Falkinham, J. O., III.** 1996. Epidemiology of infection by nontuberculous mycobacteria. Clin. Microbiol. Rev. **9**:177–215.
17. **Field, S. K., D. Fisher, and R. L. Cowie.** 2004. *Mycobacterium avium* complex pulmonary disease in patients without HIV infection. Chest **126**:566–581.
18. **Fujiwara, N., N. Nakata, S. Maeda, T. Naka, M. Doe, I. Yano, and K. Kobayashi.** 2007. Structural characterization of a specific glycopeptidolipid containing a novel *N*-acyl-deoxy sugar from *Mycobacterium intracellulare* serotype 7 and genetic analysis of its glycosylation pathway. J. Bacteriol. **189**:1099–1108.
19. **Gerwig, G. J., J. P. Kamerling, and J. F. G. Vliegenthart.** 1978. Determination of the D and L configuration of neutral monosaccharides by high-resolution capillary G.L.C. Carbohydr. Res. **62**:349–357.
20. **Hakomori, S.** 1964. A rapid permethylation of glycolipid, and polysaccharide catalyzed by methylsulfinyl carbanion in dimethyl sulfoxide. J. Biochem. (Tokyo) **55**:205–208.
21. **Heidelberg, T., and O. R. Martin.** 2004. Synthesis of the glycopeptidolipid of *Mycobacterium avium* serovar 4: first example of a fully synthetic C-mycoside GPL. J. Org. Chem. **69**:2290–2301.
22. **Howard, S. T., E. Rhoades, J. Recht, X. Pang, A. Alsup, R. Kolter, C. R. Lyons, and T. F. Byrd.** 2006. Spontaneous reversion of *Mycobacterium abscessus* from a smooth to a rough morphotype is associated with reduced expression of glycopeptidolipid and reacquisition of an invasive phenotype. Microbiology **152**:1581–1590.
23. **Kaufmann, S. H.** 2001. How can immunology contribute to the control of tuberculosis? Nat. Rev. Immunol. **1**:20–30.
24. **Khoo, K. H., D. Chatterjee, A. Dell, H. R. Morris, P. J. Brennan, and P. Draper.** 1996. Novel *O*-methylated terminal glucuronic acid characterizes the polar glycopeptidolipids of *Mycobacterium habana* strain TMC 5135. J. Biol. Chem. **271**:12333–12342.
25. **Khoo, K. H., E. Jarboe, A. Barker, J. Torrelles, C. W. Kuo, and D. Chatterjee.** 1999. Altered expression profile of the surface glycopeptidolipids in drug-resistant clinical isolates of *Mycobacterium avium* complex. J. Biol. Chem. **274**:9778–9785.
26. **Kitada, S., R. Maekura, N. Toyoshima, N. Fujiwara, I. Yano, T. Ogura, M. Ito, and K. Kobayashi.** 2002. Serodiagnosis of pulmonary disease due to *Mycobacterium avium* complex with an enzyme immunoassay that uses a mixture of glycopeptidolipid antigens. Clin. Infect. Dis. **35**:1328–1335.
27. **Kitada, S., Y. Nishiuchi, T. Hiraga, N. Naka, H. Hashimoto, K. Yoshimura, K. Miki, M. Miki, M. Motone, T. Fujikawa, K. Kobayashi, I. Yano, and R. Maekura.** 2007. Serological test and chest computed tomography findings in patients with *Mycobacterium avium* complex lung disease. Eur. Respir. J. **29**:1217–1223.
28. **Krzywinska, E., and J. S. Schorey.** 2003. Characterization of genetic differences between *Mycobacterium avium* subsp. avium strains of diverse virulence with a focus on the glycopeptidolipid biosynthesis cluster. Vet. Microbiol. **91**:249–264.
29. **Maekura, R., Y. Okuda, A. Hirotani, S. Kitada, T. Hiraga, K. Yoshimura, I. Yano, K. Kobayashi, and M. Ito.** 2005. Clinical and prognostic importance of serotyping *Mycobacterium avium-Mycobacterium intracellulare* complex isolates in human immunodeficiency virus-negative patients. J. Clin. Microbiol. **43**:3150–3158.
30. **Marras, T. K., and C. L. Daley.** 2002. Epidemiology of human pulmonary infection with nontuberculous mycobacteria. Clin. Chest Med. **23**:553–567.
31. **Maslow, J. N., V. R. Irani, S. H. Lee, T. M. Eckstein, J. M. Inamine, and J. T. Belisle.** 2003. Biosynthetic specificity of the rhamnosyltransferase gene of *Mycobacterium avium* serovar 2 as determined by allelic exchange mutagenesis. Microbiology **149**:3193–3202.
32. **McClatchy, J. K.** 1981. The seroagglutination test in the study of nontuberculous mycobacteria. Rev. Infect. Dis. **3**:867–870.
33. **McCloskey, J. A.** 1969. Mass spectrometry, p. 402. *In* J. M. Lowenstein (ed.), Methods in enzymology: lipid, vol. 14. Academic Press, New York, NY.
34. **McNeil, M., H. Gaylord, and P. J. Brennan.** 1988. *N*-formylkansosaminyl-(1-3)-2-*O*-methyl-D-rhamnopyranose: the type-specific determinant of serovariant 14 of the *Mycobacterium avium* complex. Carbohydr. Res. **177**:185–198.
35. **McNeil, M., A. Y. Tsang, and P. J. Brennan.** 1987. Structure and antigenicity of the specific oligosaccharide hapten from the glycopeptidolipid antigen of *Mycobacterium avium* serotype 4, the dominant *Mycobacterium* isolated from patients with acquired immune deficiency syndrome. J. Biol. Chem. **262**: 2630–2635.
36. **Miyamoto, Y., T. Mukai, N. Nakata, Y. Maeda, M. Kai, T. Naka, I. Yano, and M. Makino.** 2006. Identification and characterization of the genes involved in glycosylation pathways of mycobacterial glycopeptidolipid biosynthesis. J. Bacteriol. **188**:86–95.
37. **Odham, G., and E. Stenhagen.** 1972. Fatty acids, p. 211–228. *In* G. R. Waller (ed.), Biochemical application of mass spectrometry. Wiley-Interscience, New York, NY.
38. **Patterson, J. H., M. J. McConville, R. E. Haites, R. L. Coppel, and H. Billman-Jacobe.** 2000. Identification of a methyltransferase from *Mycobacterium smegmatis* involved in glycopeptidolipid synthesis. J. Biol. Chem. **275**:24900–24906.
39. **Supply, P., E. Mazars, S. Lesjean, V. Vincent, B. Gicquel, and C. Locht.** 2000. Variable human minisatellite-like regions in the *Mycobacterium tuberculosis* genome. Mol. Microbiol. **36**:762–771.
40. **Tsang, A. Y., J. C. Denner, P. J. Brennan, and J. K. McClatchy.** 1992. Clinical and epidemiological importance of typing of *Mycobacterium avium* complex isolates. J. Clin. Microbiol. **30**:479–484.
41. **Wayne, L. G., and H. A. Sramek.** 1992. Agents of newly recognized or infrequently encountered mycobacterial diseases. Clin. Microbiol. Rev. **5**:1–25.
42. **Woods, A., and J. R. Couchman.** 2001. Proteoglycan isolation and analysis, p. 10.7.1–10.7.19. *In* J. S. Bonifacino, M. Dasso, J. B. Harford, J. Lippincott-Schwartz, and K. M. Yamada (ed.), Current protocols in cell biology. Wiley Interscience, Hoboken, NJ.

THE JOURNAL OF BIOLOGICAL CHEMISTRY VOL. 283, NO. 43, pp. 28835–28841, October 24, 2008

Mycolyltransferase-mediated Glycolipid Exchange in Mycobacteria*

Received for publication, July 28, 2008, and in revised form, August 14, 2008 Published, JBC Papers in Press, August 14, 2008, DOI 10.1074/jbc.M805776200

Isamu Matsunaga[‡§], Takashi Naka[¶], Rahul S. Talekar[‖], Matthew J. McConnell[‖], Kumiko Katoh[‡§], Hitomi Nakao[‡§], Atsushi Otsuka[‡], Samuel M. Behar[‖], Ikuya Yano[¶], D. Branch Moody[‖], and Masahiko Sugita[‡§1]

From the [‡]Laboratory of Cell Regulation, Institute for Virus Research and [§]Laboratory of Cell Regulation and Molecular Network, Graduate School of Biostudies, Kyoto University, Kyoto 606-8507, Japan, [¶]Japan BCG Laboratory, Tokyo 204-0022, Japan, and [‖]Division of Rheumatology, Immunology, and Allergy, Brigham and Women's Hospital, Harvard Medical School, Boston, Massachusetts 02115

Trehalose dimycolate (TDM), also known as cord factor, is a major surface glycolipid of the cell wall of mycobacteria. Because of its potent biological functions in models of infection, adjuvancy, and immunotherapy, it is important to determine how its biosynthesis is regulated. Here we show that glucose, a host-derived product that is not readily available in the environment, causes *Mycobacterium avium* to down-regulate TDM expression while up-regulating production of another major glycolipid with immunological roles in T cell activation, glucose monomycolate (GMM). *In vitro*, the mechanism of reciprocal regulation of TDM and GMM involves competitive substrate selection by antigen 85A. The switch from TDM to GMM biosynthesis occurs near the physiological concentration of glucose present in mammalian hosts. We further demonstrate that GMM is produced *in vivo* by mycobacteria growing in mouse lung. These results establish an enzymatic pathway for GMM production. More generally, these observations provide a specific enzymatic mechanism for dynamic alterations of cell wall glycolipid remodeling in response to the transition from noncellular to cellular growth environments, including factors that are monitored by the host immune system.

Mycobacterium avium complex (MAC)[2] includes a group of acid-fast bacteria that distribute widely in natural environments, including soil, water, aerosols, and dust (1). Although less virulent than *Mycobacterium tuberculosis*, these environmental mycobacteria occasionally infect humans, especially patients infected with human immunodeficiency virus type 1, where they represent a major cause of morbidity. The incidence of clinically overt MAC infection has increased significantly in recent years, and because of the multidrug resistance evolved by the microbes, MAC infection is difficult to clear with chemotherapeutic agents. Thus, *M. tuberculosis* and MAC are now the two major groups of mycobacteria species that require further efforts for prevention and treatment. Unlike *M. tuberculosis*, which transmits primarily from individuals with active disease, epidemiologic evidence suggests that such transmission pathways are unlikely for MAC. Rather, MAC infection appears to occur when susceptible individuals are exposed to environmental MAC. These observations predict that, upon infection, environmental MAC should undergo significant adaptive changes to allow its survival and replication within the host.

Mycobacteria possess highly lipid-rich cell walls that are critical not simply for their acid-fast properties but also for their survival and replication. The cell wall contains mycolic acids, an α-alkyl-β-hydroxy fatty acid with extremely long carbon chains ($\sim C_{80}$), which are densely aligned in covalent association with the 6-position of arabinose termini of the underlying arabinogalactan sugar layer or exist as free molecules complexed to sugars, either glucose or trehalose. Arabinogalactan-linked mycolates are proposed to extend outward and interact noncovalently with carbon chains of the so-called surface-exposed glycolipids, including trehalose 6-monomycolate (TMM), trehalose 6,6′-dimycolate (TDM), and glucose 6-monomycolate (GMM), thereby forming the hydrophobic cell wall architecture that is essential for protection against chemical attack, such as reactive oxygen intermediates and hydrolytic enzymes derived from the host cells. Among the most abundant surface-exposed glycolipids is TDM that is biosynthesized from its precursor, TMM, by the mycolyltransferase activity of antigen 85 (Ag85) (2). Many biological functions have been assigned to TDM (3) that may impact on survival of mycobacteria within the host and possibly their virulence. Therefore, it is important to determine how biosynthesis of TDM and other mycolic acid-containing glycolipids is regulated by external factors. GMM exists at varied levels in the mycobacterial cell wall (4, 5). In addition to its role in cell wall barrier functions, GMM is a granuloma-forming agent in mice (6) as well as a CD1b presented antigen in humans (7).

* This work was supported, in whole or in part, by National Institutes of Health Grant R01 07155 (NIAID) (to D. B. M.). This work was also supported by grants-in-aid from scientific research on priority areas from the Ministry of Education, Culture, Sports, Science and Technology (to M. S.), grants-in-aid for scientific research B (to M. S.) and C (to I. M.) from the Japan Society for the Promotion of Science, grants from the Ministry of Health, Labour, and Welfare Research on Emerging and Re-emerging Infectious Diseases (to M. S.), and by the Burroughs Wellcome Fund (to D. B. M.). The costs of publication of this article were defrayed in part by the payment of page charges. This article must therefore be hereby marked "*advertisement*" in accordance with 18 U.S.C. Section 1734 solely to indicate this fact.

The nucleotide sequence(s) reported in this paper has been submitted to the DDBJ/GenBank™/EBI Data Bank with accession number(s) AB325677.

[1] To whom correspondence should be addressed: 53 Kawahara-cho, Shogoin, Sakyo-ku, Kyoto 606-8507, Japan. Fax: 81-75-752-3232; E-mail: msugita@virus.kyoto-u.ac.jp.

[2] The abbreviations used are: MAC, *Mycobacterium avium* complex; Ag85, antigen 85; GC-MS, gas chromatography-mass spectrometry; GMM, glucose 6-monomycolate; IL-2, interleukin-2; MALDI-TOF MS, matrix-assisted laser desorption ionization-time of flight mass spectrometry; TCR, T cell receptor; TDM, trehalose 6,6′-dimycolate; TMM, trehalose 6-monomycolate; LC-MS, liquid chromatography-mass spectrometry.

Here we identify Ag85A as an enzyme that produces GMM by transfer of mycolate to glucose. Furthermore, mechanistic studies show that glucose present in its growth environment regulates the spectrum of mycolylglycolipids made by MAC, and glucose from the host influences GMM production *in vivo* during infection of mice. Mechanistic studies showed that glucose and trehalose compete as substrates for Ag85A, linking the biosynthesis pathways of GMM and TDM.

EXPERIMENTAL PROCEDURES

Reagents and Bacteria—Chemical reagents were purchased from Nacalai Tesque (Kyoto, Japan) unless otherwise indicated. *M. avium* ATCC 35767 (serovar 4) was obtained from American Type Culture Collection (Manassas, VA). The bacteria were maintained on a plate of Middlebrook 7H10 media supplemented with 10% oleic acid/albumin/dextrose/catalase (BD Biosciences). For extraction of the total lipid fraction, the bacteria were cultured in Middlebrook 7H9 broth media (containing 0.05% Tween 80 but not glycerol) supplemented with 10% albumin/dextrose/catalase (BD Biosciences). The log phase culture was diluted with 20 volumes of 7H9 media containing various concentrations of glucose, and the culture was continued for another 5–7 days until the absorbance at 600 nm reached ~1. In some experiments, bacteria were grown in media containing either 0.01 or 0.1% glucose, and the media were replaced every day with fresh media containing the same concentrations of glucose. After 5 days, the bacteria were harvested for lipid extraction. To monitor early GMM production, bacteria were grown either in 7H9 media containing 0.01 or 0.1% glucose or in human serum and were harvested after 2, 4, 8, 18, and 24 h of culture.

Preparation of Mycolylglycolipids from MAC—Total lipids from mycobacteria were prepared as described previously (8). The total lipids were then dissolved in chloroform/methanol (C/M, 2:1, v/v), and 20 volumes of ice-cold acetone were added. After 30 min of incubation on ice, the suspension was subjected to centrifugation at 1,500 × *g* for 15 min at 1 °C, and the supernatant was carefully removed. The pellet was then washed with ice-cold acetone, and the residue was dissolved in C/M (2:1) and fractionated by TLC using an Analtech TLC plate (Newark, DE) with a solvent system of chloroform/methanol/acetone/acetic acid (90:10:10:1, v/v). GMM, TDM and TMM fractions were extracted with C/M (2:1) from the silica gels. For GMM and TDM purification, the fractions were further fractionated by TLC with a solvent system of chloroform/acetone/methanol/water (50:60:2.5:0.6, v/v). Finally, the GMM, TDM and TMM fractions were extracted with C/M (2:1), dried, and rinsed several times with methanol at room temperature to remove any residual contamination of glycopeptidolipids and phospholipids.

Matrix-assisted Laser Desorption Ionization-Time of Flight Mass Spectrometry (MALDI-TOF MS)—MALDI-TOF MS analyses of glycolipids were carried out according to the method described previously (9). Briefly, MALDI-TOF MS spectra were acquired on a Voyager DE-STR MALDI-TOF mass spectrometer (Applied Biosystems) with a pulse laser emitting at 337 nm. Samples were analyzed in the reflectron mode with an accelerating voltage operating in positive ion mode of 20 kV. As the matrix, 2,5-dihydroxybenzoic acid was used.

Gas Chromatography-Mass Spectrometry (GC-MS)—GC-MS analysis of the sugar moiety of GMM was carried out according to the method described previously (9). Briefly, GMM was hydrolyzed with 2 M trifluoroacetic acid at 120 °C for 2 h. The aqueous phase was dried, reduced with 10 mg/ml solution of $NaBD_4$ (1 M NH_4OH/C_2H_5OH, 1:1, v/v) at room temperature for 2 h, and then acetylated with acetic anhydride/pyridine (1:1, v/v) at 100 °C for 1 h. The resulting alditol acetate derivatives were analyzed by GC-MS with GCMS-QP2010 plus (Shimazu Co., Ltd., Kyoto, Japan), using a fused silica capillary column (SP-2380, 30 m × 0.25 mm inner diameter; Supelco Inc.). GC oven was operated at 50 °C for 0.5 min, and then the temperature was increased to 235 °C at a rate of 65 °C/s. The temperature was then kept at 235 °C for 12 min. Flow rate of helium gas was 44.4 cm/min.

Isolation of the Antigen 85A Gene from MAC, Preparation of the Recombinant Enzyme and Its Enzymatic Assay—The genomic DNA was isolated from the MAC strain using the Isoplant kit according to the manufacturer's instruction (Wako Pure Chemical Co. Ltd., Osaka, Japan). The gene that encoded the mature Ag85A lacking the signal sequence was amplified by PCR, using a specific primer set as follows: 5′-gga att cca tat gtt ctc gcg ccc cgg tct gcc-3′ (a sense primer, in which the NdeI restriction site is underlined) and 5′-ccg ctc gag ggt gcc ctgg ccg ttc ccg g-3′ (an antisense primer, in which the XhoI restriction site is underlined). PCR was carried out using a Takara LA-*Taq*DNA polymerase (Takara Co. Ltd., Tokyo, Japan), and the cycling conditions for PCR amplification were as follows: 94 °C, 2 min, followed by 30 cycles of 98 °C, 20 s and 72 °C, 1.5 min, and a final extension step of 72 °C, 3 min. The amplified PCR products were digested with NdeI and XhoI and ligated to a NdeI-XhoI-digested pET-21c plasmid vector (Merck). The nucleotide sequences of the Ag85A gene were determined for four isolated clones. *Escherichia coli* BL21 (DE3) was transformed with the Ag85A gene in pET-21c, and induction of protein expression was performed according to a method of Kremer *et al.* (10).

The bacteria expressing the His-tagged mature Ag85A were harvested and disrupted by sonication in ice-cold 20 mM Tris-HCl buffer (pH 7.9) containing 0.5 M NaCl and 60 mM imidazole (sonication buffer). The sonicate was centrifuged at 10,000 × *g* for 30 min at 4 °C to remove insoluble materials, and then the supernatant was applied onto a Ni^{2+}-resin column equilibrated with the sonication buffer at 4 °C. After washing the column with the sonication buffer, the recombinant Ag85A was eluted with 20 mM Tris-HCl buffer (pH 7.9) containing 0.5 M NaCl and 0.5 M imidazole. The eluate was concentrated and dialyzed against 50 mM Tris-HCl buffer (pH 7.4) containing 10% glycerol overnight at 4 °C. Protein concentration of the recombinant Ag85A preparation was determined by the Quick Start Bradford protein assay kit (Bio-Rad). Purity of the preparation was determined by SDS-PAGE and Coomassie staining.

Mycolyltransferase assays were carried out by modification of a method of Kremer *et al.* (10). Twenty μg of purified TMM was dispersed by sonication in 150 μl of 50 mM sodium phosphate buffer (pH 7.4) in the presence or absence of indicated

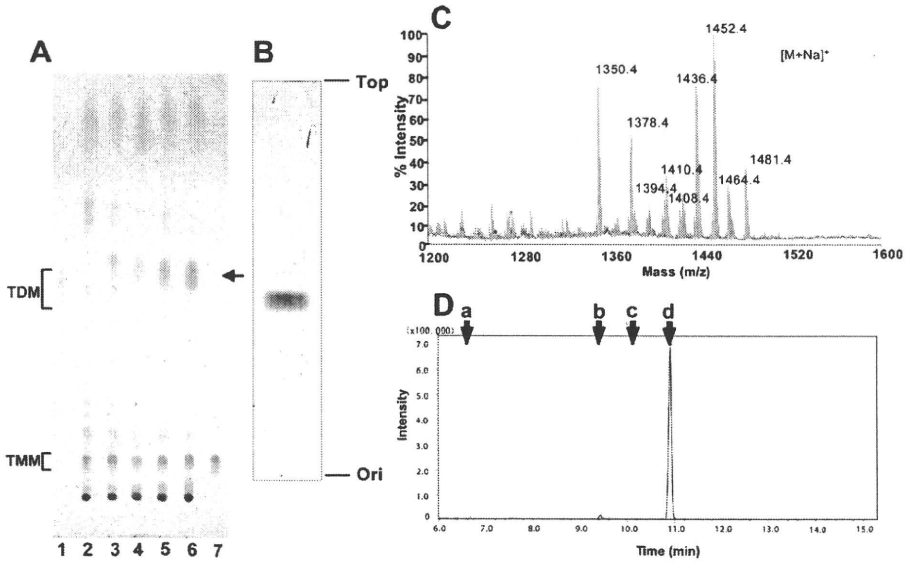

FIGURE 1. **A reciprocal production of TDM and GMM in MAC in response to glucose.** *A*, MAC was cultured in media containing 0.01% (w/v, *lane 2*), 1% (w/v, *lane 3*), 2% (w/v, *lane 4*), 5% (w/v, *lane 5*), and 10% glucose (w/v, *lane 6*), and the total lipid fractions (50 μg each) were analyzed on a TLC plate that was developed with chloroform/methanol/acetone/acetic acid (90:10:10:1, v/v). Purified TDM (*lane 1*) and TMM (*lane 7*) were used as references. Glucose dose-dependent production of a lipid species (indicated with an *arrow*) was detected. *B*, lipid species was purified and analyzed on a silica gel TLC plate that was developed with chloroform/methanol (9:1, v/v). *C*, MALDI-TOF MS profiles of the purified lipid species. *D*, GC-MS analysis of the sugar moiety of the purified lipid species. *Arrows* indicate retention times for the alditol acetate derivatives of arabinose (*a*), mannose (*b*), galactose (*c*)/ and glucose (*d*). Ion chromatogram of *m/z* 290 is shown. The retention time of the major ion corresponded with that of a glucose alditol acetate derivative.

concentration of D-glucose. The reaction was started by the addition of 50 μl of the enzyme preparation containing 50 μg of protein. After 1 h of incubation at 37 °C, the reaction was stopped by the addition of 2 ml of C/M (2:1) and 0.3 ml of distilled water. The lipids were extracted by the method of Kremer *et al.* (10) and analyzed by silica gel TLC. The lipids on the TLC plate were visualized by spraying 50% sulfuric acid and baking.

GMM Detection in Vivo—Mouse infections were carried out via the aerosol route with 10^2 *M. tuberculosis* Erdman strain with mice sacrificed after ~21 days of infection. Lungs were homogenized with beads and centrifuged at 2000 × *g* for 30 min at room temperature. The bacterial pellet was treated with 2% NaOH to disperse phospholipid bilayers, neutralized with 0.27 M phosphoric acid in phosphate buffered saline, and centrifuged at 2000 × *g* for 30 min to recover bacteria. Lipids were extracted from this mixture with three serial extractions in C/M (2:1, 1:1, and 1:2), evaporated to dryness under nitrogen, and resuspended in 1:1 C/M. These lipids were further fractionated by cold acetone precipitation to enrich for lipids that were analyzed by normal phase chromatography on a diol column. Solvent A was methanol, and solvent B was 60:40 (v/v) hexane/2-propanol. Both solvents contained 0.1% (v/v) formic acid and 0.05% (v/v) ammonium hydroxide. A binary gradient was used beginning at 5% solvent A for 3 min, linearly increasing to 40% solvent A over 5 min, holding at 40% solvent A for 6 min, linearly increasing to 100% solvent A over 2.2 min, holding at 100% solvent A for 3 min, linearly decreasing to 5% solvent A over 3.6 min, and finally holding at 5% solvent A for 3.2 min. Compounds matching the expected mass for GMM were detected at after 3.6–3.9 min of elution under these conditions. The accurate mass experiment was carried out with an Agilent 6520 Accurate Mass QTOF-LC-MS operated in the positive mode with an Agilent Technologies 1200 Series high pressure liquid chromatography system. CID-MS was carried out with a ThermoLCQ Advantage Ion Trap mass spectrometer with nano-electrospray ionization in comparison with GMM derived from *Mycobacterium fallax* (11).

GMM-specific T Cell Assays—The T cell receptor (TCR)-deficient Jurkat cells (J.RT3) reconstituted by transfection with GMM-specific, CD1b-restricted TCRs have been described previously (12). The T cells (5×10^4/well) were cocultured in 96-well microtiter plates with the C1R human B-lymphoblastoid cells (1×10^5/well) stably transfected either with CD1b (C1R/CD1b) or with empty vector alone (C1R/mock) (13) in the presence of phorbol 12-myristate 13-acetate (10 ng/ml) and indicated concentrations of lipid preparations. In some experiments, monocyte-derived dendritic cells were used as antigen-presenting cells. After 20 h, aliquots of the culture supernatants were collected, and the amount of interleukin-2 (IL-2) released into the supernatants was measured by the IL-2 ELISA kit (BD Biosciences).

RESULTS

Reciprocal Production of TDM and GMM by MAC in Response to Glucose—Glucose is an essential nutrient to living organisms, which is utilized as a source not only for energy production but also for biosynthesis of glycosylated constituents of cellular architecture. Unlike other hexose sugars, glucose is maintained at high levels in the blood and tissues of mammalian hosts. Therefore, we predicted that, upon infection into the host, MAC grown in glucose-limited environments might undergo significant alterations in glycolipid biosynthesis by exposure to host-derived glucose. To gain insights into the impact of exogenous glucose on glycolipid composition in mycobacteria, we first monitored glycolipid production by *M. avium* strain (serovar 4) that was harvested after cultivation in liquid media supplemented with different concentrations of glucose. The total lipid fraction was obtained by extracting each bacterial preparation with chloroform and methanol. The lipids were then analyzed on a TLC plate developed with a solvent system suitable for separation of chemically diverse glycolipid species (Fig. 1*A*). When grown in the presence of a trace amount of glucose (0.01%, w/v), mycobacteria produced high levels of TDM and TMM (Fig. 1*A*, *lane 2*, shown with *brackets*). As the glucose concentrations present in media were increased,

TDM production decreased, whereas the amount of TMM remained constant (Fig. 1*A*, *lanes 2–6*). Also, an increase in a discrete, unknown lipid species with a retardation factor (R_f) slightly greater than that of TDM was noted (Fig. 1*A*, *lanes 3–6*, indicated with an *arrow*). To determine the molecular identity of the unknown lipid, it was purified and subjected to TLC and MS analyses. The purified lipid was resolved as doublet bands on a TLC plate developed with a solvent system of C/M (9:1, v/v) (Fig. 1*B*). MALDI-TOF MS analysis revealed that the mass numbers of given ions were matched with those of sodium adducts of hexose monomycolate (Fig. 1*C*). Within the limits of error of the method of detection, the masses matched both in terms of the expected *m/z* of the dominant ions, the range of mass variation expected of individual molecular species of mycolate derivatives, and the absolute mass differences among the major ions, which can be accounted for by differences in carbon chain length and substitution of R groups (14). For example, *m/z* 1452.4 corresponds to the expected mass of sodium adduct of hexose monomycolate with C_{85} fatty acid and a wax ester-type R group on the meromycolate chain (Fig. 1*C*). GC-MS analysis of an alditol acetate derivative of the sugar moiety derived from the purified lipid identified glucose as the hexose group attached to mycolates (Fig. 1*D*). The doublet bands observed on a TLC plate were thus likely to represent two stereoisomers of mycolates as described previously (5, 15). Finally, the production of GMM in response to added glucose is expected based on the ability of mycobacteria to couple abundant hexose sugars at mycolyl esters (5). These results detected a reciprocal production of TDM and GMM by MAC in response to exogenous glucose without apparent alterations in the steady state levels of TMM. This experiment, carried out in live bacteria, raised the possibility that mycolyltransferases might compete for carbohydrate substrates.

Ag85 Utilized Glucose for GMM Biosynthesis—Mycobacteria-derived mycolyltransferases, known also as Ag85, catalyze the final step of TDM biosynthesis, using TMM as a substrate. Current models of the Ag85-catalyzed reaction predicted that two molecules of TMM are captured in the two substrate-binding pockets of the enzyme, and the mycolyl acyl group of the TMM substrate bound in one substrate-binding pocket (donor site) is transferred to the other TMM substrate bound in the other pocket (acceptor site), resulting in generation of one molecule of TDM and one molecule of trehalose (Fig. 2*A*) (2, 16). Although GMM can be an abundant structure in the cell wall and functions to activate T cells and form granulomas, its mechanism of synthesis was unknown. We hypothesized that GMM biosynthesis could be catalyzed by Ag85 if glucose, instead of TMM, occupied the acceptor site (Fig. 2*B*). To address this possibility, we made recombinant Ag85A enzyme from the *M. avium* strain (serovar 4), and we performed *in vitro* enzymatic reaction experiments. To accomplish this, we first carried out PCR from the genome of the MAC strain as a template, and isolated the Ag85A gene that encoded the mature protein lacking the signal sequence. DNA sequencing of the isolated gene revealed that three nucleotides were altered as compared with the previously reported Ag85A gene derived from *M. avium* serovar 1 strain (17), but the deduced amino acid sequences were identical in both strains. We then constructed an expression plasmid in which the initiation codon was placed at the 5′-end and the sequence encoding a His tag was attached in frame at the 3′-end of the isolated Ag85A gene. The His-tagged enzyme was expressed in *E. coli* and affinity-purified by Ni^{2+}-charged resin column chromatography. The purified material was resolved as a single band with an apparent molecular mass of ~33 kDa on a Coomassie-stained SDS-polyacrylamide gel, consistent with its being the Ag85A protein (Fig. 3*A*). Incubation of TMM *in vitro* in the presence of this

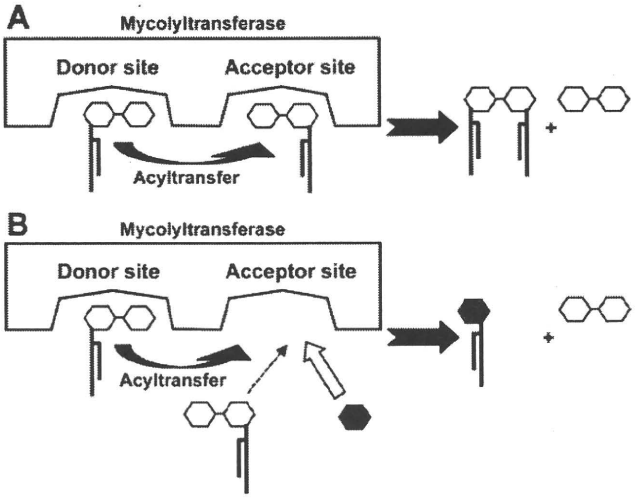

FIGURE 2. **Proposed scheme for TDM (*A*) and GMM (*B*) production catalyzed by mycolyltransferase.** In *model A*, both the donor site and the acceptor site of the enzyme interact with TMM, resulting in TDM formation. In *model B*, a glucose substrate competes against a TMM substrate for access to the acceptor site. When glucose is readily available, glucose rather than TMM preferentially gain access to the site, resulting in production of GMM.

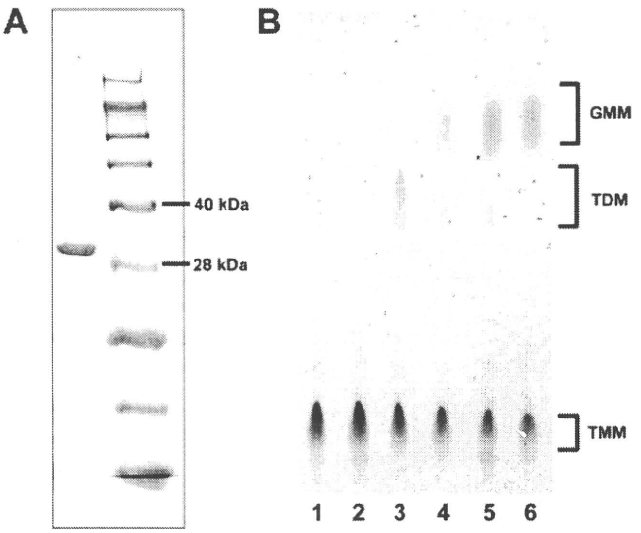

FIGURE 3. **TDM-GMM exchange mediated by recombinant Ag85A.** *A*, purified MAC Ag85A (*left lane*) and a size marker (*right lane*) were resolved on a Coomassie-stained SDS-polyacrylamide gel. Positions for the 40- and 28-kDa marker proteins are indicated. *B*, enzymatic reactions were performed at 37 °C at conditions indicated below, and the lipids were extracted from the reaction mixtures, followed by analysis on a TLC plate. *Lane 1*, Ag85A and TMM with 5% glucose (w/v), 0 h of incubation; *lane 2*, heat-inactivated (100 °C, 3 min) Ag85A and TMM with 5% glucose (w/v), 1 h of incubation; *lanes 3–6*, Ag85A and TMM either with 0.2% (w/v) glucose (*lane 4*), 1% glucose (w/v) (*lane 5*), and 5% (w/v) glucose (*lane 6*) or without glucose (*lane 3*), 1 h of incubation.

enzyme preparation resulted in generation of TDM (Fig. 3*B*, *lane 3*), confirming the mycolyltransferase activity exerted by the recombinant protein. Strikingly, addition of glucose to this reaction condition resulted in decreased TDM production in a dose-dependent manner, which was associated with an increase in GMM (Fig. 3*B*, *lanes 3–6*). GMM synthesis was completely abrogated when heat-inactivated enzyme was used (Fig. 3*B*, *lane 2*). This further confirmed that GMM was produced enzymatically by the mycolyltransferase activity of Ag85A but not as a result of nonenzymatic hydrolysis. These results indicate that Ag85A mediates synthesis of GMM. In this molecular model, we propose that TMM and glucose compete for access to the acceptor site of the Ag85A, and the enzyme preferentially catalyzes biosynthesis of GMM, rather than TDM, when glucose is readily available (Fig. 2*B*). The substrate selection by the mycolyltransferase would likely provide a molecular basis for the glucose-dependent TDM-GMM exchange detected in cultured MAC.

GMM Production Occurs at a Physiological Glucose Concentration—The observations made above have established an enzymatic pathway for GMM production in live mycobacteria that are grown in the presence of high levels of exogenous glucose. However, it remains to be addressed whether mycobacteria can produce GMM under physiological concentrations of glucose present in mammalian hosts, which is maintained at ~100 mg/dl (0.1% w/v). To address this issue, we measured GMM production by mycobacteria cultured in liquid media with a glucose concentration comparable with that in the host. The MAC culture was started in the presence of either 0.01 or 0.1% glucose, and every 24 h, the culture media were replaced with fresh media to maintain the glucose concentrations at constant levels. After 5 days of culture, the bacteria were harvested, and the total lipids were extracted. Subsequently, methanol-insoluble lipids were isolated from these total lipids, followed by separation on TLC plates (Fig. 4*A*). Although TDM production was readily detected in both cultures, GMM production was detected only in the presence of 0.1% glucose (Fig. 4*A*, *lane 2*) but not in the presence of 0.01% glucose (*lane 1*). This was also confirmed by T cell-based assays (Fig. 4*B*) in which Jurkat T cells expressing specific TCRs recognizing GMM in the context of CD1b molecules were used. Incubation of the T cells with CD1b-expressing cells (C1R/CD1b) in the presence of the total lipids from the 0.1% glucose-containing culture resulted in dose-dependent IL-2 production by the T cells, demonstrating high levels of antigenicity when growing at physiological glucose concentrations (Fig. 4*B*, *upper panel*). The specific response was not observed when CD1b-negative cells (C1R/mock) were used as antigen-presenting cells, supporting that the response was CD1b-restricted.

We then addressed how quickly induction of GMM production occurred after exposure to 0.1% glucose. MAC was cultured either in liquid media containing 0.01% (Fig. 5*A*) or 0.1% (*B*) or in human serum (*C*), and the bacteria were harvested at 2, 4, 8, 18, and 24 h. GMM production was observed as early as 8 h after the start of the culture both in 0.1% glucose-containing media and in human serum but not in media containing 0.01% glucose. These observations suggest that GMM production can occur quickly after exposure to high levels of glucose presumably as a result of competitive substrate selection by preexisting mycolyltransferases.

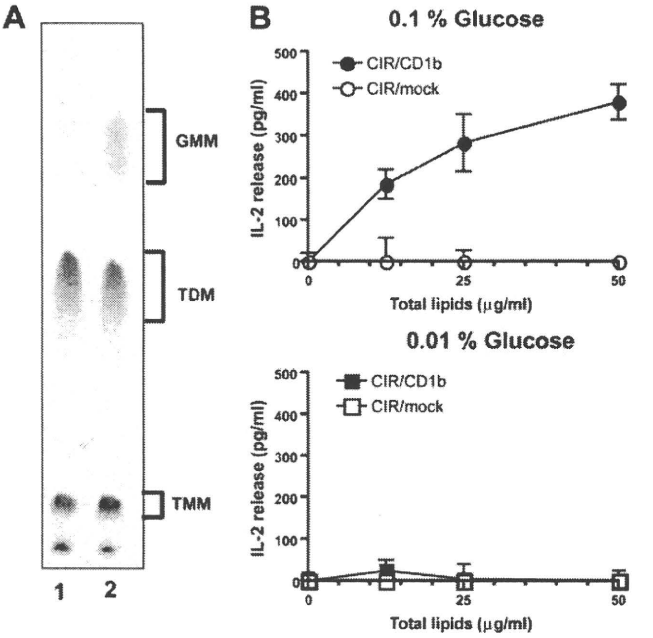

FIGURE 4. **GMM production by mycobacteria cultured at a physiological glucose concentration.** *A*, MAC was cultured in liquid media containing either 0.01 or 0.1% glucose, and the culture media were replaced with fresh media every day to maintain the glucose concentrations. After 5 days, the bacteria were harvested, and the total lipids were extracted. The methanol-insoluble fraction was then obtained from 100 μg of each total lipid preparation and analyzed by TLC. *B*, GMM-specific, CD1b-restricted TCR-expressing Jurkat T cells were cocultured with either C1R/CD1b or C1R/mock in the presence of different concentrations of the total lipids derived from the 0.1% glucose-containing (*upper panel*) and the 0.01% glucose-containing (*lower panel*) cultures. The T cell response was assessed by measuring IL-2 released into the media.

GMM Production Occurs in Mycobacteria-infected Tissues—A previous study detected GMM comigrating lipids can be derived from *Mycobacterium leprae*, raising the possibility that GMM is produced by mycobacteria in tissues (5). However, the chemical structures of such candidate glycosyl mycolates could not be directly determined, and it remained unknown whether *M. tuberculosis* produces GMM during infection. Therefore, we infected CH3 mice with *M. tuberculosis* Erdman strain and isolated mycobacteria directly from the lungs after ~3 weeks of infection. Bacteria were enriched from lung preparations by centrifugation and treatment with weak base to disperse lung tissue. The resulting preparations contained predominantly mycobacterial lipids when analyzed by LC-MS (data not shown). By comparing total *M. tuberculosis* lipids from lung with an *M. fallax* GMM standard in LC-MS experiments, we analyzed the *in vivo* derived lipids that nearly copurified with the GMM standard. Mass measurements with an Accurate Mass QTOF capable of mass resolution of 10 ppm detected an ion at 1317.2577 in lung-derived lipids (Fig. 6*A*). Both the absolute *m/z* and the isotope ratios matched the predicted masses of an ammonium adduct of a GMM carrying a C_{78} α-mycolic acid within expected error (C_{84}, $H_{162}O_8$, C_{78} GMM, expected *m/z* 1317.2613). Further supporting the identification of this ion as GMM, mycolic acid derivatives are characteristically synthe-